Coordination Chemistry Reviews 253 (2009) 2056–2069

Contents lists available at ScienceDirect

Coordination Chemistry Reviews

journal homepage: www.elsevier.com/locate/ccr

Review

NMR studies on the electronic structure of one-electron oxidized complexes of iron(III) porphyrinates

Akira Ikezaki [a], Yoshiki Ohgo [a,b], Mikio Nakamura [a,b,c,*]

[a] Department of Chemistry, School of Medicine, Toho University, Ota-ku, Tokyo 143-8540, Japan
[b] Research Center for Materials with Integrated Properties, Toho University, Funabashi, 274-8510, Japan
[c] Division of Chemistry, Graduate School of Science, Toho University, Funabashi 274-8510, Japan

Contents

ARTICLE INFO

Article history:
Received 26 October 2008
Accepted 6 January 2009
Available online 13 January 2009

Keywords:
Porphyrin
Iron(III)
One-electron oxidation
Radical cation
Iron(IV)
NMR spectroscopy

ABSTRACT

This review describes the relationship between the NMR chemical shifts and electronic structures of one-electron oxidized products of iron(III) porphyrins such as iron(III) porphyrin radical cations or iron(IV) porphyrins. In the case of the former complexes, the iron(III) ions are classified into four types; (i) high-spin (S = 5/2), (ii) mixed high- and intermediate-spin (S = 5/2, 3/2), (iii) low-spin with the $(d_{xy})^2(d_{xz}, d_{yz})^3$ ground state, and (iv) low-spin with the $(d_{xz}, d_{yz})^4(d_{xy})^1$ ground state. In the case of the latter complexes, they mostly have Fe^{IV}=O bonds. There is only one iron(IV) complex that has no Fe^{IV}=O bond. The complexes classified as above exhibit unique NMR chemical shifts. Thus, the NMR spectroscopy serves a quite useful tool to determine the fine electronic structures of the one-electron oxidized iron(III) porphyrin complexes.

Abbreviations: DMAP, 4-(*N*,*N*-dimethylamino)pyridine; 4-MePy, 4-methylpyridine; 4-CNPy, 4-cyanopyridine; HIm, imidazole; 2-MeIm, 2-methylimidazole; 4,5-Cl_2Im, 4,5-dichloroimidazole; ^{t}BuNC, *tert*-butylisocyanide; PyNO, pyridine *N*-oxide; 4-MePyNO, 4-methylpyridine *N*-oxide; 3,5-Me_2PyNO, 3,5-dimethylpyridine *N*-oxide; Por, dianion of porphyrin; TArP, dianion of 5,10,15,20-tetraarylporphyrins; TRP, dianion of 5,10,15,20-tetraalkylporphyrins where R is ethyl(Et), propyl(Pr), or isopropyl(^{i}Pr); ORTPP, dianion of 2,3,7,8,12,13,17,18-octaalkyl-5,10,15,20-tetraphenylporphyrins where R is methyl(M) or ethyl(E); Fe(Por)X and $[Fe(Por)L_2]^+$, iron(III) porphyrin where X is an anionic ligand and L is a neutral ligand; Por•, porphyrin radical cation with total charge-1; $Fe(Por^•)X^+$, $Fe(Por^•)XY$, and $[Fe(Por^•)L_2]^{2+}$, iron(III) porphyrin radical cation where X and Y are anionic ligands and L is a neutral ligands; (Fe=O)(Por), oxo-iron(IV) porphyrins; $Fe(Por)X_2$, iron(IV) porphyrins with anionic ligand X. Structures of these porphyrin dianions are given in Scheme 1.

* Corresponding author at: Department of Chemistry, School of Medicine, Toho University, Ota-ku, Tokyo 143-8540, Japan. Tel.: +81 337624151; fax: +81 354935430.
E-mail address: mnakamu@med.toho-u.ac.jp (M. Nakamura).

0010-8545/$ – see front matter © 2009 Elsevier B.V. All rights reserved.
doi:10.1016/j.ccr.2009.01.003

1. Introduction

High-valent iron porphyrin complexes have been extensively studied both experimentally and theoretically since they play important roles in the catalytic cycles of a number of heme enzymes [1–5]. One-electron oxidation of iron(III) porphyrins should form either iron(IV) porphyrin or iron(III) porphyrin radical cations. Actually, however, most of the papers reported previously have shown the formation of iron(III) porphyrin radical cations. These radical species give characteristic ^{1}H NMR spectra, where some of the signals appear extraordinary upfield or downfield positions due to the presence of unpaired electron in the porphyrin orbitals [6]. In iron(III) porphyrins, the central iron(III) ion can adopt various electronic structures including the high-spin (S = 5/2), low-spin (S = 1/2), and intermediate-spin (S = 3/2) state [7–14]. Some complexes exhibit the mixed spin state such as S = 1/2, 3/2 [15–19], S = 1/2, 5/2 [20–23], and S = 3/2, 5/2 [24–26]. Furthermore, each spin state has different electron configuration as is well exemplified in the low-spin complexes which adopt either the $(d_{xy})^2(d_{xz}, d_{yz})^3$ or the $(d_{xz}, d_{yz})^4(d_{xy})^1$ electronic ground state [6,8,27,28]. Similarly, at least two electronic ground states exist even in the intermediate-spin complexes, i.e. $(d_{xy})^2(d_{xz}, d_{yz})^2(d_z2)^1$ and $(d_{xz}, d_{yz})^3(d_{xy})^1(d_z2)^1$ [29]. The unpaired electron in the porphyrin orbital cannot be independent of the paramagnetic iron center. It could interact with the paired and/or unpaired electrons in the iron 3d orbitals. Consequently, the ^{1}H NMR spectra should be affected by the spin states and electron configurations of the iron(III) ions. In the case of iron(IV) porphyrins, the iron could adopt S = 0, S = 1 or S = 2 spin state though no examples have ever been reported for the S = 0 and S = 2. The unpaired electrons in the S = 1 complexes can delocalize to the porphyrin ring by the interactions with the porphyrin π orbitals to give characteristic ^{1}H NMR spectra [6]. For these reasons, ^{1}H NMR spectroscopy has been used as a powerful tool to determine the fine electronic structures of iron porphyrins. In this review article, we describe the characteristic features of the NMR spectra of one-electron oxidized products of iron(III) porphyrins such as iron(III) porphyrin radical cations and iron(IV) porphyrins. Structures and abbreviations of porphyrin dianions are given in Scheme 1.

2. Effects of orbital interactions on the NMR chemical shifts

2.1. Orbital symmetry

It is very important to understand the iron–porphyrin orbital interactions to reveal the relationship between the NMR parameters and the electronic structures of the complexes. Thus, before going into the electronic structure of one-electron oxidized complexes, let us briefly survey the iron-porphyrin orbital interactions. Fig. 1 shows the frontier orbitals of porphyrin with D_{4h} symmetry. Among these orbitals, the occupied $3e_g$ and vacant $4e_g^*$ orbitals can interact with the iron d_π(d_{xz} and d_{yz}) orbitals. If the complex in question has half-occupied d_π orbitals as in the case of the low-spin iron(III) complexes with the $(d_{xy})^2(d_{xz}, d_{yz})^3$ ground state, the unpaired electron can delocalize to the porphyrin ring by the d_π–$3e_g$ interactions especially to the pyrrole β-C atoms because the $3e_g$ orbitals have relatively large coefficient at these carbon atoms as shown in Fig. 1 [6,8,28,30–35]. Fig. 2 shows how unpaired electron in the metal delocalizes to the porphyrin ring and induces the contact shift to protons [27,35]. As shown in Fig. 2(a) and (b), the spin density at the sp^2 hybridized carbon atoms signified as C_X induces the upfield shift of the directly bonded proton, i.e. C_X–H, and the downfield shift of the methyl and methylene protons such as C_X–CH_3 and C_X–CH_2–R by the spin polarization mechanism. If phenyl group attaches to the C_X atom, then the *o*- and *p*-H signals move upfield while the m-H signal shifts downfield as shown in Fig. 2(c). If the negative spin is induced for some reasons to the C_X atom, the signals for all the protons mentioned above shift to the opposite directions as is revealed from Fig. 2(d) to (e).

In principle, all the frontier orbitals of porphyrin except for the e_g orbitals are orthogonal to any of the iron d orbitals and thus there should be no interaction other than the d_π–$3e_g$ and d_π–$4e_g^*$ interactions. Actually, however, porphyrin rings are flexible and they are easily deformed by the steric and electronic effects of the peripheral substituents and the axial ligands [8]. Typical deformation modes frequently encountered are ruffling, saddling, and doming as given in Fig. 3 [36–40]. The ruffling indicates that the *meso*-carbon atoms deviate from the mean porphyrin plane up and down alternately while the saddling indicates that the β carbon atoms deviate

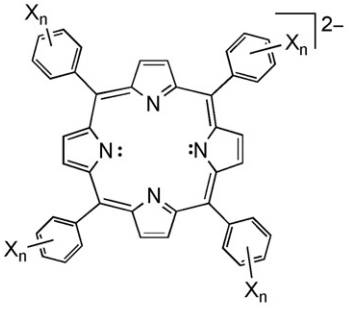

X_n	Porphyrin dianion
H	TPP
3-Me	3-MeTPP
4-Me	4-MeTPP
4-OMe	4-OMeTPP
2,4,6-$(OMe)_2$	4-OMeTPP
2,6-F_2	2,6-F_2TPP
2,4,6-Me_3	TMP
2,3,5,6-Me_4	TDP

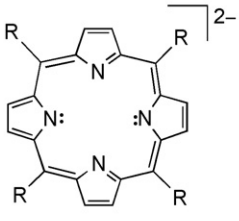

R	Porphyrin dianion
Et	TEtP
Pr	T^nPrP
^{i}Pr	T^iPrP

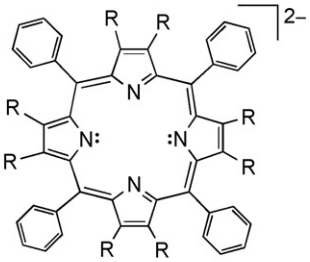

R	Porphyrin dianion
Me	OMTPP
Et	OETPP

Scheme 1. Structures and abbreviations of porphyrin dianions.

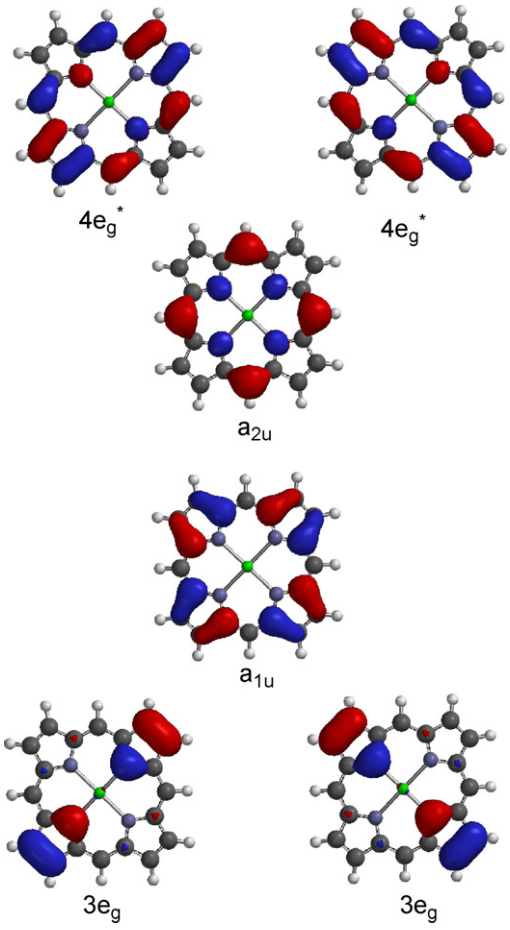

Fig. 1. Frontier orbitals of D_{4h} porphyrin.

Table 1
Correlation table for the molecular orbitals of metalloporphyrin[a].

	D_{4h} planar	D_{2d} ruffled	D_{2d} saddled	C_{4v} domed
Metal				
$d_{x^2-y^2}$	b_{1g}	b_1	b_2	b_1
d_{z^2}	a_{1g}	a_1	a_1	a_1
d_{zx}, d_{yz}	e_g	e	e	e
d_{xy}	b_{2g}	b_2	b_1	b_2
Porphyrin				
$4e_g^*$	$4e_g^*$	e	e	e
a_{1u}	a_{1u}	b_1	b_1	a_2
a_{2u}	a_{2u}	b_2	b_2	a_1
$3e_g$	$3e_g$	e	e	e

[a] Adapted from Ref. [41,42].

similarly. The doming is a typical structure of five-coordinate iron porphyrin complexes where iron is placed out of the plane defined by the four nitrogen atoms of the pyrrole rings. If the porphyrin ring deforms in a ruffled or saddled fashion, some metal–porphyrin orbital interactions can be allowed, which are originally forbidden in a planar D_{4h} complex. Table 1 shows the symmetry presentation of metal and porphyrin orbitals in six-coordinate planar D_{4h}, ruffled D_{2d}, and saddled D_{2d} complexes as well as five-coordinate domed C_{4v} complexes [41,42]. As shown in Table 1, the metal d_π(d_{xz} and d_{yz}) orbitals can interact with the porphyrin e_g orbitals in planar D_{4h} complexes. The interaction takes place regardless of the deformation mode of the porphyrin ring since these orbitals have the same symmetry not only in D_{4h}(planar) complexes but also in D_{2d}(ruffled, saddled) and C_{4v}(domed) complexes. If the complex deforms in a ruffled fashion, the interactions should take place between the iron d_{xy} and porphyrin a_{2u} and also between the iron $d_{x^2-y^2}$ and porphyrin a_{1u} orbital; the d_{xy} and a_{2u} orbitals are signified as b_2 while the $d_{x^2-y^2}$ and a_{1u} orbitals are signified as b_1 in ruffled D_{2d} complexes [43–45]. Similarly, saddling switches on the $d_{x^2-y^2}$–a_{2u} and the d_{xy}–a_{1u} interactions; the $d_{x^2-y^2}$ and a_{2u} orbitals are represented as b_2 while the d_{xy} and a_{1u} orbitals are represented as b_1 in saddled

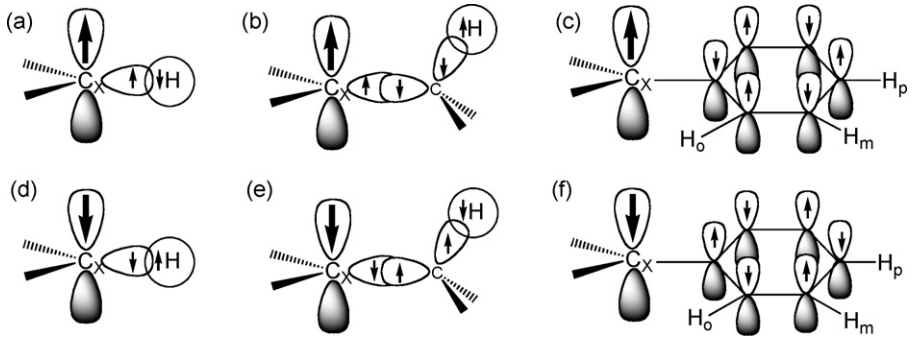

Fig. 2. Effects of the positive spin at the sp^2 hybridized carbon atom signified as C_X on the ^1H NMR chemical shifts of (a) C_X–H, (b) C_X–CH_3 or C_X–CH_2–R, and (c) H_o, H_m, and H_p signals. Effects of the negative spin at C_X on the chemical shifts of (d) C_X–H, (e) C_X–CH_3 or C_X–CH_2–R, and (f) H_o, H_m, and H_p signals.

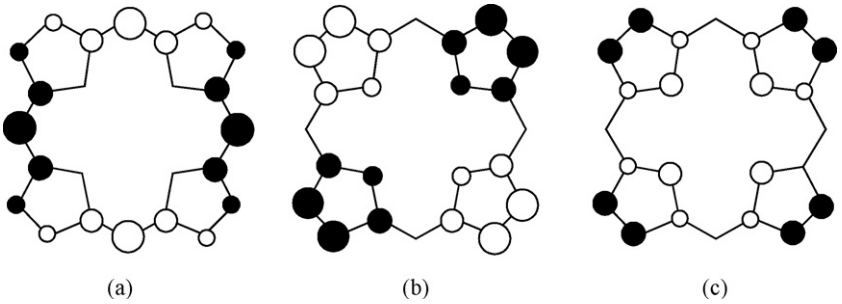

Fig. 3. Major deformation modes of porphyrin. (a) Ruffled deformation, (b) saddled deformation, and (c) domed deformation. Open circles represent atoms above the least-squares plane and the filled circles represent atoms below the plane. Adapted from Ref. [40].

Table 2
^{1}H NMR chemical shifts of $[Fe(TRP)L_2]^{\pm}$ in CD_2Cl_2 at 223 K[a].

L	Pyrrole-H			*meso*-C		
	^{n}Pr	^{c}Pr	^{i}Pr	^{n}Pr	^{c}Pr	^{i}Pr
HIm	−21.5	−18.7	0.1	73.1	97.1	331.6
DMAP	−16.7	−14.3	4.0	130.5	127.4	402.2
2-MeIm	−8.2	−8.5[b]	5.6[b]	[c]	190.4[b]	434.0[b]
CN^-	−3.5	4.3	12.3	336.1	386.7	639.6
3-MePy	4.5	7.3	14.7	470.0	431.6	702.5
Py	7.1	8.4	14.9	526.5	448.9	728.6
4-CNPy	13.0	14.9	15.6	814.7	680.1	917.5
^{t}BuNC	12.7	14.7	12.9	[c]	[c]	[c]

[a] Adapted from Refs. [48,60].
[b] Averaged value.
[c] Not observed.

D_{2d} complexes [46,47]. In the case of the five-coordinate domed C_{4v} complexes, both the iron d_z^2 and porphyrin a_{2u} orbitals have the same symmetry, a_1, and thus the interaction can be expected between these orbitals [41].

2.2. Six-coordinate ruffled D_{2d} complex

Table 2 lists the ^{1}H and ^{13}C NMR chemical shifts of a series of low-spin iron(III) complexes $[Fe(TRP)L_2]^{\pm}$ taken in CD_2Cl_2 solution at 298 K. Among various complexes listed in Table 2, $[Fe(T^nPrP)(HIm)_2]^+$ clearly adopts the $(d_{xy})^2(d_{xz}, d_{yz})^3$ ground state [48]. The major interaction in this complex occurs between the half-occupied iron d_π and porphyrin $3e_g$ orbitals. Consequently, the unpaired electron is delocalized to the porphyrin ring especially to the pyrrole β-C atoms and induces the upfield shift of the pyrrole-H signal; i.e. −21.5 ppm at 223 K. Since the $3e_g$ orbital has zero coefficient at the *meso*-C atoms, the *meso*-C signal is considered to appear quite close to the diamagnetic position. Actually, however, it is observed rather upfield position, 73 ppm, due to the spin polarization from the neighboring α-C atoms. Dipolar term should contribute to some extent to the upfield shift of the *meso*-C signal; the peripheral and axial signals shift upfield and downfield, respectively, in the $(d_{xy})^2(d_{xz}, d_{yz})^3$ type complexes [49].

If axial ligand has low-lying π* orbital, then the d_π orbitals are stabilized and the complex tends to adopt the $(d_{xz}, d_{yz})^4(d_{xy})^1$ ground state [48,50–62]. If the porphyrin ring is intrinsically ruffled due to the introduction of bulky alkyl groups at the *meso* positions, then the d_{xy} orbital is destabilized due to the symmetry allowed d_{xy}–a_{2u} interaction. Thus, the complex also tends to form the $(d_{xz}, d_{yz})^4(d_{xy})^1$ ground state [8]. Typical example showing the $(d_{xz}, d_{yz})^4(d_{xy})^1$ ground state is $[Fe(T^iPrP)(4\text{-}CNPy)_2]^+$ [48], where the axial ligand has low-lying π* orbitals and the porphyrin core is highly ruffled. This complex has a considerable amount of spin density on the *meso*-C atoms; note that the a_{2u} orbital has large coefficient at the *meso*-C atoms as shown in Fig. 1. As a result, the *meso*-C signal appears at an extremely downfield position, i.e. 918 ppm at 223 K. The data in Table 2 also indicate that the pyrrole-H signal appears rather downfield, 15.6 ppm. Since the a_{2u} orbital has zero coefficient at the pyrrole β-C atoms, the downfield shift should be ascribed to the dipolar contribution. In fact, clear evidence has been obtained that the dipolar effects shift the peripheral and axial signals to the downfield and upfield positions, respectively, in the $(d_{xz}, d_{yz})^4(d_{xy})^1$ type complexes [49].

2.3. Six-coordinate saddled D_{2d} complex

Saddling switches on the iron($d_{x^2-y^2}$)–porphyrin(a_{2u}) interaction. In saddle shaped iron(III) porphyrins, high-spin complexes have half-occupied $d_{x^2-y^2}$ orbital. Thus, the $d_{x^2-y^2}$–a_{2u} interaction induces the positive spin on the pyrrole-N and *meso*-C atoms. Consequently, the *meso*-C signal appears downfield [63]. Although there is no example of six-coordinate saddle shaped $[Fe(OETPP)L_2]^+$ showing the pure high-spin state, the chemical shift of the *meso*-C signal is estimated to be 168 ppm [63], which is ca. 50 ppm more downfield than the corresponding signal of diamagnetic Zn(OETPP) [64]. If the complex adopts the intermediate-spin state, the interaction is expected between the filled a_{2u} and empty $d_{x^2-y^2}$ orbital. The interaction could induce the negative spin to the a_{2u} orbital by the spin polarization mechanism proposed by Cheng et al. [65]. As a result, the *meso*-C signal should move upfield. Table 3 shows the ^{13}C NMR chemical shifts of saddled $[Fe(OETPP)L_2]^+$, where Int(%) indicates the population of the S = 3/2 in the mixed S = 3/2 and S = 5/2 spin state [63]. The axial ligands are arranged in the ascending order of the S = 3/2 character. As the spin state changes from the mixed S = 5/2, S = 3/2 in the bis(4-MePyNO) complex to the pure S = 3/2 in the bis(THF) complex, the *meso*-C signal continuously moves upfield from −19 to −269 ppm. The results indicate that the a_{2u}–$d_{x^2-y^2}$ interaction controls the chemical shift of the *meso*-C signal in the mixed S = 5/2 and S = 3/2 spin system.

2.4. Five-coordinate domed C_{4v} complex

In five-coordinate iron(III) porphyrins, the iron(III) ion is placed out of the porphyrin plane. In such a case, the interaction occurs between the iron d_z2 and porphyrin a_{2u} orbital as pointed out by Cheng et al., which induces positive spin on the *meso*-C atoms [41]. In fact, the chemical shift of the *meso*-C signal in five-coordinate high-spin Fe(TPP)Cl is 495 ppm while that of six-coordinate high-spin $[Fe(TPP)(DMSO)_2]^+$ is 13 ppm [66]. In the ^{1}H NMR spectrum of Fe(TPP)Cl, the positive spin at the *meso*-C atoms induce the upfield shift of the *o*- and *p*-H signals and the downfield shift of the *m*-H signals. The chemical shifts are 6.2, 3.8 ppm for *o*-H, 12.6, 12.0 ppm for *m*-H and 5.8 ppm for *p*-H.

Fig. 4 shows the relationships between *meso*-C and pyrrole-H chemical shifts in a large number of five- and six-coordinate high-spin iron(III) complexes such as Fe(Por)X and $[Fe(Por)L_2]^+$(Por = TArP, TRP; X = Cl^-, Br^-, I^-; L = PyNO, 4-MePyNO, 3,5-Me_2PyNO, DMSO, DMF) [67]. As is clear from Fig. 4, the

Table 3
^{13}C NMR chemical shifts (δ ppm)of $[Fe(OETPP)L_2]^+$ taken in CD_2Cl_2 at 298 K[a].

Ligand	Pyrrole				*Meso*-Ar					Int (%)
	α	β	C_α	C_β	*meso*	*ip*	*o*	*m*	*p*	
4-MePyNO[b]	598	601	−2	190	−19	257	66	126	127	42
3,5-Me_2PyNO[b]	504	498	−14	191	−40	257	52	126	126	55
PyNO	555	512	−10	191	−63	278	38	125	125	51
DMSO	485	398	−24	186	−139	307	−4	122	122	66
DMF	419	250	−43	190	−221	338	−49	121	117	87
MeOH	409	239	−45	199	−211	343	−57	121	116	89
THF	394	215	−55	215	−269	354	−74	118	116	100

[a] Adapted from Ref. [63].
[b] The assignment of the α and β could be reversed.

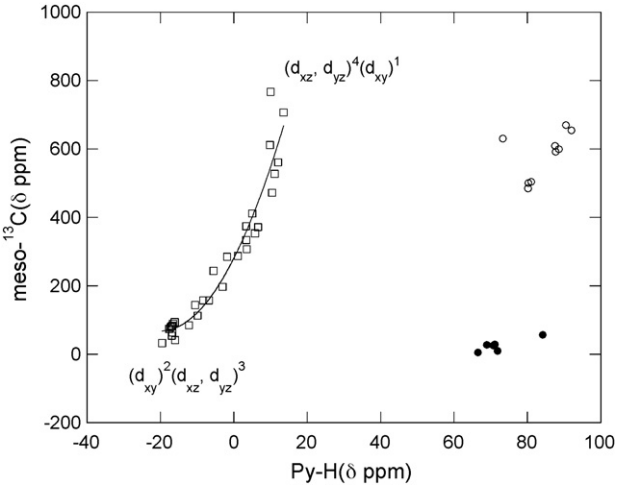

Fig. 4. Relationship between pyrrole-H and *meso*-^{13}C chemical shifts in CD_2Cl_2 solutions at 298 K. High-spin six-coordinate, high-spin five-coordinate, and low-spin six-coordinate complexes are signified by filed circle, open circle and open square, respectively. Adapted from Ref. [67].

chemical shifts of the *meso*-C signals in five-coordinate high-spin complexes are quite different form those in six-coordinate high-spin complexes although the pyrrole-H chemical shifts are not much different among them. The results suggest that the *meso*-C chemical shift is quite useful to discriminate the coordination structure of iron(III) porphyrin complexes. Rivera and co-workers have applied this method to determine the coordination structure of heme proteins [68]. They have used ^{13}C labeled δ-aminolevulinic acid as precursors for the biosynthetic preparation of ^{13}C-labeled protoheme IX. In the case of wild-type sperm whale myoglobin reconstituted with ^{13}C-labeled heme, the *meso*-C signals appear at ca. −80 ppm while those in H64V mutant resonate near 280 ppm. Since these heme proteins are known to adopt the six- and five-coordinate high-spin state, respectively, it is clear that the chemical shift of the *meso*-C signal can be a good probe to determine the coordination structure of high-spin heme proteins. By applying this method to a recently discovered heme protein from *Shigella dysenteriae*(ShuT), Rivera and co-workers have unambiguously determined that the heme is five-coordinate [68].

3. Iron(III) porphyrin radical cations

One-electron oxidation of iron(III) porphyrins produces either iron(III) porphyrin cation radicals or iron(IV) porphyrins depending mainly on the nature of axial ligands. In this section, the formation and NMR spectra of iron(III) porphyrin radical cations will be described.

3.1. High-spin iron(III) porphyrin radical cations

Goff and co-workers electrochemically oxidized a series of Fe(TPP)X where X is anionic ligands such as F^-, Cl^-, Br^-, I^-, ClO_4^- etc. and found that the one-electron oxidation potentials are quite insensitive to the axial ligands; the first oxidation potentials are ca. 1.1 V for all the complexes examined [69]. Consequently, these oxidized species are characterized as iron(III) porphyrin radical cations, Fe(TPP•)X$^+$. One of the characteristic features in ^{1}H NMR spectrum of this complex is that the pyrrole-H signal appears at an extremely downfield as that of starting high-spin Fe(TPP)Cl; they are 80.1 and 66.1 ppm for Fe(TPP)Cl and Fe(TPP•)Cl$^+$, respectively [70]. The other characteristic features are the chemical shifts of the *meso*-phenyl protons; they are 37.6, 34.4 ppm for *o*-H, −12.4 ppm for *m*-H, and 29.5 ppm for *p*-H. The large downfield shift of the pyrrole-H signal suggests that the iron $d_{x^2-y^2}$ orbital is half-occupied, which in turn indicates that the iron(III) ion is in the high-spin state. The large downfield shift of the *o*- and *p*-H signals together with the large upfield shift of the *m*-H signals suggest that the *meso*-C atoms have large amount of negative spin as shown in Fig. 2(f). Note that the a_{2u} radical with the positive spin at the *meso*-C atoms should shift the phenyl-H signals to the opposite directions as shown in Fig. 2(e) [69–71]. Thus, the ^{1}H NMR spectrum of Fe(TPP•)Cl$^+$ is indicative of the antiferromagnetic coupling between radical spin and metal spins. In fact, the Mössbauer and susceptibility studies of the solid sample indicate that the complex shows a strong antiferromagnetic coupling between the S = 5/2 iron(III) ion and the S = 1/2 porphyrin radical to lead to an overall S = 2 spin state [72–74]. The X-ray crystal structure of [Fe(TPP•)Cl]$SbCl_6$ reveals that the crystal lattice consists of discrete Fe(TPP•)Cl$^+$ and $SbCl_6^-$ ions where the porphyrin core is strongly S_4 ruffled [73]. Fe(TDP)Cl is similarly oxidized to form Fe(TDP•)Cl$^+$. The pyrrole-H signal appears at 72 ppm at 217 K. The upfield shifts of *o*-CH_3 signals at −8.0 and −10.3 ppm in Fe(TDP•)Cl$^+$ correspond with the downfield shifts of the *o*-H signals in Fe(TPP•)Cl$^+$, suggesting that both Fe(TPP•)Cl$^+$ and Fe(TDP•)Cl$^+$ adopt the same electronic structure [75].

While the *meso*-phenyl signals of Fe(TPP)Cl exhibit large isotropic shifts on one-electron oxidation, the isotropic shift of the *meso*-H signal is rather reduced in Fe(OEP)Cl [70]; the *meso*-H signals appear at −54 and −18 ppm for Fe(OEP)Cl and Fe(OEP•)Cl$^+$, respectively. Similarly, the isotropic shifts of the CH_2 signals are also reduced on going from Fe(OEP)Cl to Fe(OEP•)Cl$^+$; they are 43.1 and 39.5 ppm for the former and 30.5 and 29.6 ppm for the latter complex. Reduced isotropic shifts in Fe(OEP•)Cl$^+$ is explained in terms of the electron removal from the a_{1u} orbital; a_{1u} orbital has large coefficient at the pyrrole α-C atoms as shown in Fig. 1. Thus, the unpaired electron in the a_{1u} orbital in Fe(OEP•)Cl$^+$ is delocalized to the pyrrole α-C atoms and should shift the *meso*-H signal to the downfield positions. However, the NMR chemical shifts can also be explained in terms of the weak antiferromagnetic coupling of the a_{2u} radical with the metal spins [6]; the a_{2u} orbital can interact with the iron d_{z^2} orbital in five-coordinate C_{4v} complexes. The antiferromagnetic coupling between iron(III) and a_{2u} radical spins is most explicitly observed in the analogous iron(III) octaethyloxophlorin radical, Fe(OEPO•)Br [76]. Because of the large negative spin at the *meso*-C atoms, the *meso*-H signals resonate at extremely downfield positions, i.e. 344 and 232 ppm. Table 4 lists the chemical shifts of some iron(III) porphyrin radical cations together with those of the precursors. These data indicate that the complexes carrying aryl groups at the *meso* positions exhibit similar chemical shifts. Thus, these complexes are classified as high-spin iron(III) radical cations where a_{2u} radical spin antiferromagnetically couples with metal spins [77,78].

^{13}C NMR spectroscopy is quite useful to determine the electronic structures of iron(III) porphyrin complexes [8,28,79]. Little is known, however, on the ^{13}C NMR spectra of iron(III) porphyrin radicals although their importance and usefulness to reveal the electronic structure of radical species was pointed out many years ago [80]. This is because some ^{13}C NMR signals in radical species are quite difficult to observe due to their extreme broadness. In fact, the ^{13}C NMR spectrum of Fe(TPP•)Cl$^+$ exhibits only four signals at 1050, 958, 137, and 8.7 ppm. No *meso*-C signal is observed even by the use of *meso*-^{13}C(99% ^{13}C) enriched Fe(TPP•)Cl$^+$. Hoshino and Nakamura have determined the ^{13}C NMR chemical shifts of Fe(TPP•)Cl$^+$ by the titration method [81]. As shown in Fig. 5, addition of only 0.075 equiv of Fe(TPP•)Cl$^+$ to the CD_2Cl_2 solution of Fe(TPP)Cl shifts the *meso*-C signal from 495 to 376 ppm. Furthermore, the half-height width ($W_{1/2}$) increases from 306 to 2530 Hz. When 0.23 equiv of the radical is added, the *meso* signal with $W_{1/2}$ = 3890 Hz appears at 48.0 ppm. The signal is no longer observed after the addition of 0.3 equiv of the radical. Since the electron exchange between

Table 4
^{1}H NMR chemical shifts of high-spin iron(III) porphyrin radical cations Fe(Por)X$^+$ and their parent complexes Fe(Por)X where X is halides[a] taken at ambient temperatures.

Complexes	Pyrrole			*meso*-Phenyl			Ref.
	H	α-CH_2	α-CH_3	*o*-H	*m*-H	*p*-H	
Fe(OEP•)Cl$^+$	–	30.5 29.6	–	−18[b]	–	–	[70]
Fe(TPP•)Cl$^+$	66.1	–	–	37.6 34.4	−12.4	29.5	[70]
Fe(TDP•)Cl$^+$	68.0	–	–	(−8.0) (−10.3)	(2.0)	13.7	[75]
Fe(4-OMeTPP•)Cl$^+$	59.9	–	–	48.1	−9.8	(−5.7)	[70]
Fe(3-MeTPP•)Cl$^+$	68.7	–	–	44.5 42.6	−13.0 (5.9)	37	[74]
Fe(4-MeTPP•)Cl$^+$	64.8	–	–	48.0	−14.7	(−30.5)	[74]
Fe(2,6-F_2TPP•)Cl$^+$	85.5	–	–	−140[c]	−3.5 −4.5	16.0	[77]
Fe(OMTPP•)Cl$^+$	–		69.9 63.0	39.7 36.9	−11.0 12.5	31.7	[78]
Fe(OETPP•)Cl$^+$	–	71.2 56.1 24.7 16.6	–	37.6 34.9	−10.1 −11.5	28.8	[78]
Fe(OEP)Cl	–	43.1 39.5	–	−54[b]	–	–	[70]
Fe(TPP)Cl	80.1	–	–	6.2 3.8	12.6 12.0	5.8	[78]
Fe(TDP)Cl	79.7	–	–	(6.2) (3.7)	(3.8) (3.3)	8.0	[113]
Fe(4-OMeTPP)Cl	79.6	–	–	ca. 6	12.8 11.9	(5.2)	[70]
Fe(2,6-F_2TPP)Cl	80.0	–	–	−78.5[c] −81.0[c]	13.5 11.8	7.0	[77]
Fe(OMTPP)Cl	–	–	51.1	11.3 8.6	12.5 12.2	7.4	[78]
Fe(OETPP)Cl	–	49.0 34.8 32.1 20.1	–	11.5 9.1	12.4 12.2	7.5	[78]

[a] Data in parentheses are the chemical shifts of the methyl signals.
[b] *meso*-H.
[c] *ortho*-F.

Fe(TPP)Cl and Fe(TPP•)Cl$^+$ is fast on the ^{1}H NMR timescale, the observed chemical shift δ_{obs} is expressed by Eq. (1) in the presence of t equiv of the radical, where δ_N and δ_R are the chemical shifts of the carbon atoms in Fe(TPP)Cl and Fe(TPP•)Cl$^+$, respectively. Fig. 6 shows the plots of δ(obs) against $1/(1+t)$, from

$$\delta(\text{obs}) = \delta_R + \frac{\delta_N - \delta_R}{1+t} \quad (1)$$

which the chemical shifts of the *meso*-C, pyrrole α-C, and *o*-C are determined to be −1910, 2230, and −721 ppm, respectively. Other four signals at 1050, 958, 137, and 8.7 ppm are assigned to the pyrrole β-C, *ipso*-C, *m*-C, and *p*-C, respectively. These values are summarized in Table 5 together with those of Fe(TPP)Cl. The large upfield shift of the *meso*-C signal is a direct indication of antiferromagnetic coupling of this species [81]. Because of the negative spin at the *meso*-C and pyrrole-N atoms, the neighboring pyrrole α-C signal appears at an extraordinary downfield position, i.e. 2230 ppm.

3.2. Mixed high-spin and intermediate-spin iron(III) porphyrin radical cations

If the field strengths of axial ligands are weak, both five- and six-coordinate iron(III) porphyrin complexes adopt the mixed high-spin and intermediate-spin state [9]. If the field strengths of anionic ligands are extremely weak such as $[Ag(Br_6CB_{11}H_6)_2]^-$, the five-coordinate complex adopts an essentially pure intermediate-spin state [10,11]. Similarly, if the porphyrin ring is highly deformed as in the case of ruffled T^{i}PrP and saddled OETPP, the correspond-

Table 5
^{13}C NMR chemical shifts of Fe(TPP•)Cl$^+$ and Fe(TPP)Cl determined in CD_2Cl_2 solution at 298 K[a].

Complexes	py-α	py-β	*meso*	*ip*	*o*	*m*	*p*	Ref.
Fe(TPP•)Cl$^+$	*2230*	1050	*−1910*	958	*−721*	137	8.7	[81]
Fe(TPP)Cl	1204	1321	495	−71.7	400, 417	148, 152	143	[81,111,112]

[a] Chemical shifts written in italic were obtained by the titration method.

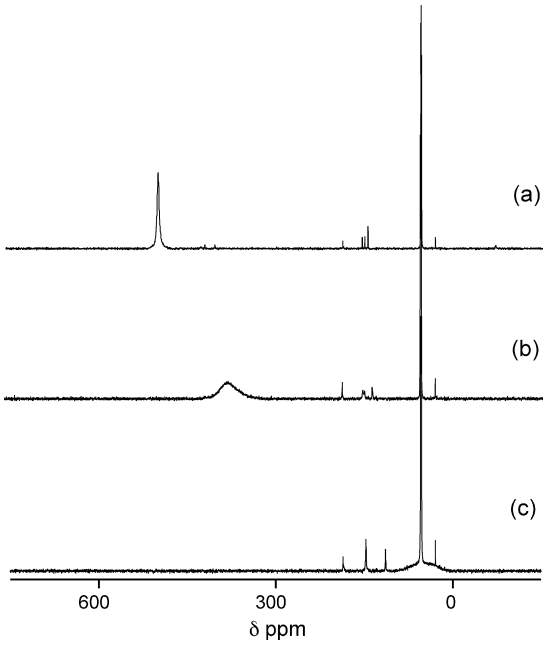

Fig. 5. Spectroscopic change of *meso*-^{13}C enriched Fe(TPP)Cl on addition of *meso*-^{13}C enriched radical cationic Fe(TPP•)Cl$^+$ in CD_2Cl_2 solution at 298 K: (a) 0.00, (b) 0.075, and (c) 0.23 equiv. Adapted from Ref. [81].

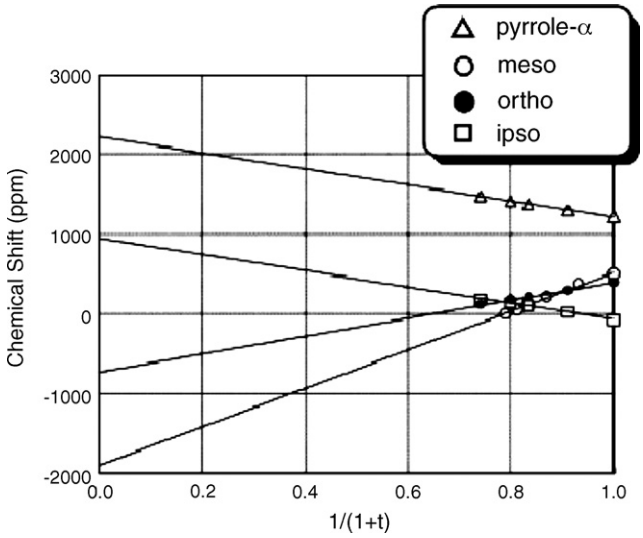

Fig. 6. Plots of chemical shifts of *meso*-^{13}C signals in Fe(TPP)Cl against $1/(1+t)$ where t (equiv) is the amount of Fe(TPP•)Cl$^+$ added to the CD_2Cl_2 solution of Fe(TPP)Cl at 298 K. The ^{13}C chemical shifts in Fe(TPP•)Cl$^+$ are determined from the y-intercepts. Adapted from Ref. [81].

ing complexes exhibit the pure intermediate-spin state even if the field strengths of the axial ligands are not very weak [12–14]. Thus, the complexes such as Fe(T^{i}PrP)X and Fe(OETPP)X are known to adopt the quite pure intermediate-spin state if X = ClO_4^- or I^- [14,82]. Similarly, six-coordinate complexes such as [Fe(T^{i}PrP)L_2]$^+$ and [Fe(OETPP)L_2]$^+$ exhibit the intermediate-spin state if weak oxygen ligands such as THF and dioxan coordinate axially [13,63,83]. In the case of [Fe(OETPP)L_2]$^+$, even the coordination of weak nitrogen bases such as 4-CNPy leads to the formation of an essentially pure intermediate-spin state [15].

Electrochemical or chemical oxidation of mixed high-spin and intermediate-spin complexes also yields iron(III) porphyrin radical cations. Typical example is Fe(TPP•)$(ClO_4)_2$. The X-ray crystal structure reveals that, unlike the highly ruffled Fe(TPP•)Cl$^+$ core, the Fe(TPP•)$(ClO_4)_2$ core is planar [73]. The ^{1}H NMR spectrum shows the pyrrole-H signal at 31.4 ppm, and *o*-, *m*-, and *p*-H signals at, −19.3, 34.7, and −12.9 ppm, respectively, at 298 K [71,74]. Thus, the signs of the chemical shifts of *meso*-phenyl signals are opposite to those of high-spin iron(III) porphyrin radical cations such as Fe(TPP•)Cl$^+$. The NMR data suggest that the *meso*-C atoms have a large amount of positive spin as shown in Fig. 2(e), which indicates that there is no appreciable antiferromagnetic coupling in this complex. The result is understandable because the a_{2u} orbital is orthogonal to any of the iron d orbitals in planar D_{4h} complex. The solution magnetic moment of this complex ranges from 4.4 to 5.2 μ_B depending on the samples prepared separately [71]. The NMR spectrum of analogous Fe(TPP•)$(SO_3CF_3)_2$ shows the pyrrole-H signal at 43.9 ppm at 305 K and *o*-, *m*-, and *p*-H signals at, −17.1, 31.3, and −11.3 ppm, respectively, at 309 K [71]. Table 6 lists the chemical shifts of one-electron oxidized Fe(TPP•)X_2 together with those of Fe(TPP)X adopting the mixed S = 5/2 and S = 3/2 spin state. The data in Table 6 indicate that the pyrrole-H signals in both Fe(TPP•)X_2 and Fe(TPP)X move upfield as the axial ligand X changes from $CF_3SO_3^-$

Table 6
^{1}H NMR chemical shifts of mixed high-spin and intermediate-spin iron(III) porphyrin radical cations Fe(Por•)XYand their parent complexes Fe(Por)X where X and Y are anionic ligands[a].

Complexes	T (K)	Solvent	Pyrrole-H	*meso*-Phenyl			Ref.
				o-H	*m*-H	*p*-H	
Fe(TPP•)Cl(ClO_4)	299	CD_2Cl_2	66.1	37.6, 34.4	−12.3	29.5	[70]
Fe(TPP•)$(SO_3CF_3)_2$	309	CD_2Cl_2	43.9[b]	−17.1	31.3	−11.3	[71]
Fe(TPP•)$(ClO_4)_2$	298	CD_2Cl_2	31.4	−19.3	34.7	−12.9	[71]
Fe(TMP•)$(ClO_4)_2$	294	CD_2Cl_2	18.7	(20)	55	(12.5)	[84]
	195	CD_2Cl_2	−22.5	(32.2)	90.9	(19.7)	[84]
	195	CD_2Cl_2/CD_3OD[c]	ca. 100[d]	(41)	122, 119	(27)	[84]
	294	Toluene-d_8	39.6	(21.1)	58.2	(12.3)	[84]
	195	Toluene-d_8	61	(39)	115	(23)	[84]
Fe(TPP)Cl	298	CD_2Cl_2	80.1	6.2, 3.8	12.6, 12.0	5.8	[78]
Fe(TPP)(SO_3CF_3)	302	$CDCl_3$	39.3	9	12.5	7.5	[71]
Fe(TPP)ClO_4	302	$CDCl_3$	13.0	9.2	11.9	7.7	[71]
Fe(TMP)ClO_4	295	CD_2Cl_2	−12.5	(3.35)	10.52	(3.86)	[84]
	195	CD_2Cl_2/CD_3OD[b]	47.9	(4.82)	11.9	(5.96)	[84]

[a] Data in parentheses are the chemical shifts of the methyl signals.
[b] Data at 305 K.
[c] Fe(TMP•)(ClO_4) is converted to high-spin [Fe(TMP•)$(CD_3OD)_2$](ClO_4) in CD_2Cl_2/5% CD_3OD solution.
[d] Three signals are observed at 93.1, 102, 108 ppm.

to ClO_4^-. Thus, the pyrrole-H chemical shifts of these complexes are mainly determined by the contribution of the S = 3/2 [71]. The data in Table 6 also indicate that the pyrrole-H signal of Fe(TPP•)X_2 appears more downfield than that of corresponding Fe(TPP)X for both X = ClO_4^- and $CF_3SO_3^-$, meaning that the electron removal from the porphyrin ring rather stabilizes the S = 5/2 in the mixed S = 5/2, 3/2 iron(III) complexes [71]. It should be noted that the electronic structure of Fe(TPP•)$(ClO_4)_2$ in solution seems to be different from that in the solid, because the solid sample of Fe(TPP•)$(ClO_4)_2$ exhibits the magnetic moment 6.5 μ_B, which suggests the presence of ferromagnetic coupling between radical spin and high-spin iron(III) spins [74].

One-electron oxidation of Fe(TMP)ClO_4 by Fe$(ClO_4)_3$ gives iron(III) porphyrin radical cation Fe(TMP•)$(ClO_4)_2$. The chemical shifts are very much sensitive to solvent and temperature [84]. In CD_2Cl_2 solution at 294 K, the ^{1}H NMR spectrum shows the pyrrole-H signal at 18.7 ppm and *o*-CH_3, *m*-H, and *p*-CH_3 signals at 20, 55, and 12.5 ppm, respectively. Thus, the complex has large positive spin at the *meso*-C atoms as shown in Fig. 2(e) due to the formation of the a_{2u} radical. As the temperature is lowered, the pyrrole-H signal moves upfield while the *meso*-phenyl signals shift further downfield. At 195 K, the pyrrole-H signal is observed at −22.5 ppm while the *o*-CH_3, *m*-H, and *p*-CH_3 signals appear at 32.2, 90.9, and 19.7 ppm, respectively. The NMR spectroscopic behavior suggests that the interaction between a_{2u} radical and iron(III) spins is fairly weak and that the spin state of iron(III) changes from the mixed S = 5/2, S = 3/2 at 294 K to the mainly S = 3/2 at 195 K. In toluene-d_8 solution, however, the pyrrole-H signal moves downfield from 39.6 ppm at 294 K to 61 ppm at 195 K. The result can be explained in terms of the increase in population of the high-spin state in non-polar toluene-d_8 solution [85]. By the addition of methanol-d_4 to the CD_2Cl_2 solution of Fe(TMP•)$(ClO_4)_2$, the pyrrole-H signal shows a large downfield shifts from −22.5 to ca. 100 ppm at 195 K. Thus, Fe(TMP•)$(ClO_4)_2$ is converted to [Fe(TMP•)$(CD_3OD)_2$]$(ClO_4)_2$ which is in a high-spin state with the a_{2u} porphyrin radical cation, where a_{2u} radical is almost independent of the high-spin iron(III). The chemical shifts of these complexes are listed in Table 6. For comparison, the chemical shifts of high-spin radical cation Fe(TPP•)Cl(ClO_4) are also listed in Table 6.

3.3. Low-spin iron(III) porphyrin racial cation

Although direct oxidation of six-coordinate low-spin iron(III) porphyrin complexes is unsuccessful, addition of axial ligand(L) to S = 5/2 or mixed S = 3/2, S = 5/2 iron(III) porphyrin radical cations such as Fe(TPP•)Cl^+ and Fe(TMP•)$(ClO_4)_2$ permits generation of oxidized six-coordinate low-spin complexes expressed as [Fe(Por•)L_2]$^{2+}$ if the axial ligand is neutral. Depending on the nature of axial ligands and deformation mode of porphyrin ring, low-spin iron(III) adopts either the $(d_{xy})^2(d_{xz}, d_{yz})^3$ or the $(d_{xz}, d_{yz})^4(d_{xy})^1$ ground state. Thus, the interaction of porphyrin radical with these two types of iron(III) ions should be different.

3.3.1. Iron(III) with the $(d_{xy})^2(d_{xz}, d_{yz})^3$ electron configuration

Addition of imidazole to a CD_2Cl_2 solution of Fe(TPP•)Cl^+ at 235 K yields the corresponding bis(HIm) complex, [Fe(TPP•)$(HIm)_2$]$^{2+}$ [86]. This complex shows the pyrrole-H signal at −40.1 ppm, while the *o*-, *m*-, and *p*-H signals appear at −31.7, 30.4, and −22.1 ppm, respectively, at 235 K [86]. The NMR data suggest that the oxidized bis(HIm) complexes are best described as low-spin iron(III) porphyrin radical cations, where radical spin is in the a_{2u} orbital. Solution magnetic moment for the analogous [Fe(*p*-OMeTPP•)$(HIm)_2$]$^{2+}$ is 2.8 ± 0.2 μ_B, suggesting that the radical spin does not strongly couple with the metal spins. The result is indicative of the planar porphyrin structure where a_{2u} orbital is orthogonal to any of the iron d orbitals. In the case of low-spin iron(III) porphyrins, the pyrrole-H chemical shifts are affected by the electronic ground state of low-spin iron(III). While the low-spin complexes with the $(d_{xy})^2(d_{xz}, d_{yz})^3$ ground state exhibit the pyrrole-H signals rather upfield due to the d_π–$3e_g$ interactions, those with the $(d_{xz}, d_{yz})^4(d_{xy})^1$ ground state exhibit them near their diamagnetic positions as shown in Table 2. Thus, it is clear that the iron(III) ion in [Fe(TPP•)$(HIm)_2$]$^{2+}$ adopts the low-spin state with the $(d_{xy})^2(d_{xz}, d_{yz})^3$ ground state.

Addition of imidazole ligands such as 2-MeIm and HIm to CD_2Cl_2 solution of sterically hindered Fe(TDP•)Cl^+ at 195 K forms [Fe(TDP•)$(2\text{-MeIm})_2$]$^{2+}$ and [Fe(TDP•)$(HIm)_2$]$^{2+}$ [75]. Fig. 7 shows the ^{1}H NMR spectra of [Fe(TDP•)$(2\text{-MeIm})_2$]$^{2+}$ and [Fe(TDP•)$(HIm)_2$]$^{2+}$ together with those of Fe(TDP•)Cl^+ and

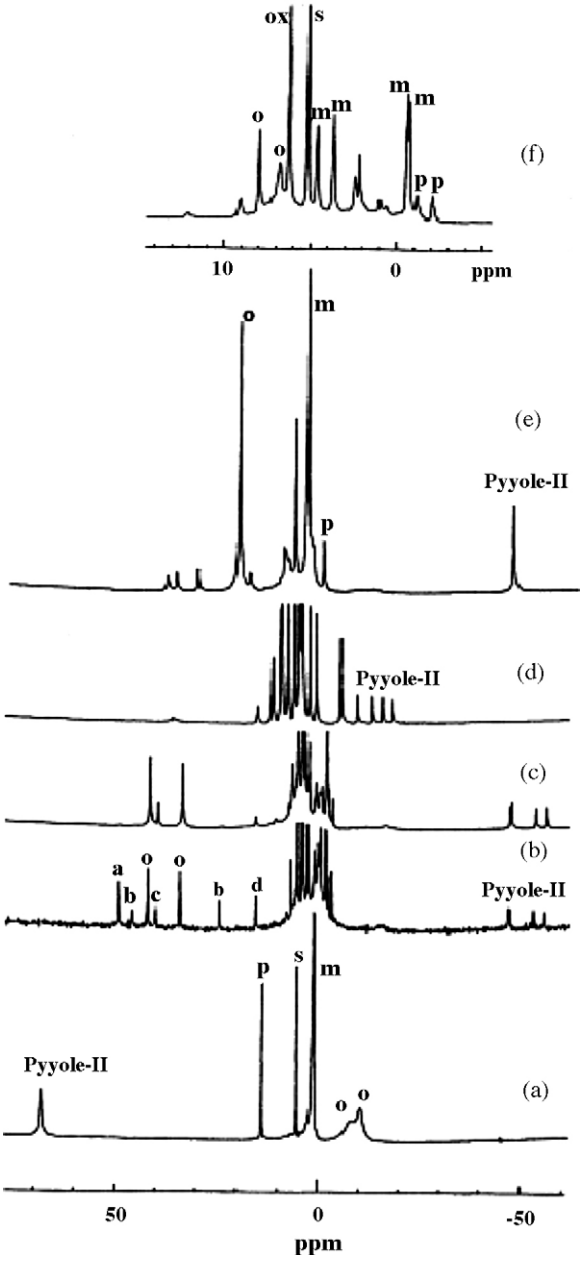

Fig. 7. ^{1}H NMR spectra taken in CD_2Cl_2 solution at 217 K. (a) Fe(TDP•)Cl^+. (b) [Fe(TDP•)$(2\text{-MeIm})_2$]$^{2+}$. (c) [Fe(TDP•)$(2\text{-MeIm})_2$]$^{2+}$ where all the ^{1}H of 2-MeIm except N–H are deuterated. (d) [Fe(TDP)$(2\text{-MeIm})_2$]$^+$ obtained after standing [Fe(TDP•)$(2\text{-MeIm})_2$]$^{2+}$ at 298 K for 10 s. (e) [Fe(TDP•)$(HIm)_2$]$^{2+}$. Signal assignments: Symbols *o*, *m*, and *p* indicate the *o*-CH_3, *m*-CH_3, and *p*-H signals, respectively. Symbols a, b, and c indicate the imidazole signals. Adapted from Ref. [75].

Table 7
^{1}H NMR chemical shifts of low-spin iron(III) porphyrin radical cations $[Fe(Por^{\bullet})L_2]^{2+}$ and their parent complexes $[Fe(Por)L_2]^+$ where L is neutral ligand[a].

Complexes	T (K)	Pyrrole-H	*Meso*			Ref.
			o-H α-H	*m*-H β-H	*p*-H	
$[Fe(TArP^{\bullet})L_2]^{2+}$						
$[Fe(TPP^{\bullet})(HIm)_2]^{2+}$	235	−40.1	−31.7	30.4	−22.1	[86]
$[Fe(4\text{-}OMeTPP^{\bullet})(HIm)_2]^{2+}$	235	−32.7	−36.3	24.8	(12.9)	[86]
$[Fe(2,4,6\text{-}OMeTPP^{\bullet})(HIm)_2]^{2+}$	243	−40.4	(12.8)	26.7	(9.5)	[86]
$[Fe(TDP^{\bullet})(HIm)_2]^{2+}$	217	−49.1	(19.0)	(2.2)	−1.8	[75]
$[Fe(TDP^{\bullet})(2\text{-}MeIm)_2]^{2+}$	217	−49.5[b]	(22.8)[b]	(1.8)[b]	−1.6[b]	[75]
$[Fe(TMP^{\bullet})L_2]^{2+}$						
$[Fe(TMP^{\bullet})(HIm)_2]^{2+}$	213	−53.2	(20.1)	52.1	(7.0)	[91]
$[Fe(TMP^{\bullet})(4,5\text{-}Cl_2Im)_2]^{2+}$	213	−25.6	n.d.	24.8	(4.0)	[91]
$[Fe(TMP^{\bullet})(^t BuNC)_2]^{2+}$	213	4.64	(2.66)	6.78	(2.24)	[91]
$[Fe(TRP^{\bullet})L_2]^{2+}$						
$[Fe(TEtP^{\bullet})(HIm)_2]^{2+}$	223	−36.0	*230.9*	*15.5*	–	[90]
$[Fe(TPrP^{\bullet})(HIm)_2]^{2+}$	223	−34.1	*232.6*	*−8.8*	–	[90]
$[Fe(T^iPrP^{\bullet})(HIm)_2]^{2+}$	223	−20.4	*42.4*	*9.0*	–	[90]
$[Fe(TEtP^{\bullet})(2\text{-}MeIm)_2]^{2+}$	223	−33.7[b]	*206.6*[b]	*14.4*[b]	–	[90]
$[Fe(TPrP^{\bullet})(2\text{-}MeIm)_2]^{2+}$	223	−30.9[b]	*208.2*[b]	ca. *−7*	–	[90]
$[Fe(T^iPrP^{\bullet})(2\text{-}MeIm)_2]^{2+}$	223	−21.7[b]	*47.9*[b]	*9.4*[b]	–	[90]
$[Fe(TArP)L_2]^+$						
$[Fe(TPP)(HIm)_2]^+$	298	−16.8	5.1	6.2	6.3	[113]
$[Fe(4\text{-}OMeTPP)(HIm)_2]^+$	298	−16.6	5.0	5.8	(3.2)	[113]
$[Fe(2,4,6\text{-}OMeTPP)(HIm)_2]^+$	298	−16.8	(1.7)	5.1	(3.8)	[113]
$[Fe(TDP)(HIm)_2]^+$	298	−16.4	(0.80)	(1.6)	6.1	[113]
$[Fe(TMP)L_2]^+$						
$[Fe(TMP)(HIm)_2]^+$	298	−16.8	(0.9)	6.0	(1.6)	[113]
$[Fe(TMP)(4,5\text{-}Cl_2Im)_2]^+$	298	−9.4	(2.2)	10.0	(3.1)	[113]
$[Fe(TMP)(^t BuNC)_2]^+$	298	7.1	(5.5)	18.2	(4.2)	[113]
$[Fe(TRP)L_2]^+$						
$[Fe(TEtP)(HIm)_2]^+$	223	−21.2	*1.3*	*−1.2*	–	[90]
$[Fe(TPrP)(HIm)_2]^+$	223	−20.9	*2.4*	*−1.0*	–	[90]
$[Fe(T^iPrP)(HIm)_2]^+$	223	0.6	*16.5*	*3.9*	–	[90]
$[Fe(TEtP)(2\text{-}MeIm)_2]^+$	223	−9.4	*16.7*	*1.1*	–	[90]
$[Fe(TPrP)(2\text{-}MeIm)_2]^+$	223	−8.8	*19.8*	*n.d.*	–	[90]
$[Fe(T^iPrP)(2\text{-}MeIm)_2]^+$	223	5.6[b]	*21.2*[b]	*5.4*[b]	–	[90]

[a] Data in parentheses are the chemical shifts of the methyl signals. The chemical shifts of the mesoalkyl groups are given in italic letter.
[b] Averaged value.

$[Fe(TDP^{\bullet})(2\text{-}MeIm)_2]^+$. As shown in Fig. 7(b), $[Fe(TDP^{\bullet})(2\text{-}MeIm)_2]^{2+}$ exhibits four pyrrole signals around −50 ppm at 217 K. Similarly, four *o*-CH_3, four *m*-CH_3, and two *p*-H signals appear at 22.8, 1.8, and −1.6 ppm in average, respectively. The number of the split signals indicate that the rotation of the coordinating 2-MeIm is hindered on the ^{1}H NMR time scale to form C_2 structure, where the axial ligands align perpendicularly along the C_{meso}–Fe–C_{meso} axes above and below the porphyrin ring as in the case of the corresponding low-spin iron(III) porphyrins [87–89]. Since the large downfield shift of the *o*-CH_3 signals correspond to the large upfield shift of the *o*-H signal in analogous $[Fe(TPP^{\bullet})(HIm)_2]^{2+}$, it is clear that $[Fe(TDP^{\bullet})(2\text{-}MeIm)_2]^{2+}$ adopts the same electronic structure as that of $[Fe(TPP^{\bullet})(HIm)_2]^{2+}$, i.e. low-spin iron(III) with the $(d_{xy})^2(d_{xz}, d_{yz})^3$ ground state. The chemical shifts of low-spin iron(III) porphyrin radical cations $[Fe(TArP^{\bullet})L_2]^{2+}$ are listed in Table 7 together with those of the corresponding low-spin iron(III) porphyrins $[Fe(TArP)L_2]^+$.

Low-spin iron(III) porphyrin radical cations carrying alkyl groups at the *meso* positions, $[Fe(TRP^{\bullet})L_2]^{2+}$(R = Et, ^{n}Pr, ^{i}Pr; L = HIm, 2-MeIm), have been obtained similarly by the addition of axial ligands to the CD_2Cl_2 solutions of $Fe(TRP^{\bullet})Cl^+$ at 195 K [90]. Fig. 8 shows the ^{1}H NMR spectra of $[Fe(TEtP^{\bullet})(HIm)_2]^{2+}$ and $[Fe(T^iPrP^{\bullet})(2\text{-}MeIm)_2]^{2+}$ taken in CD_2Cl_2 solution at 223 K [54]. As compared with $[Fe(TArP^{\bullet})L_2]^{2+}$, the pyrrole-H signals appear more downfield. The most characteristic feature is that these complexes exhibit the *meso* α-H signals at extremely downfield positions. For example, the *meso* α-H signals of $[Fe(T^nPrP^{\bullet})(HIm)_2]^+$ moves

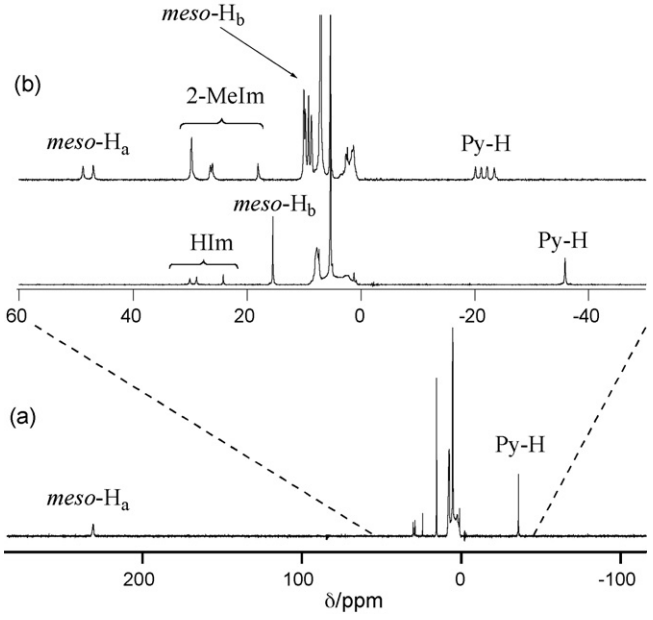

Fig. 8. ^{1}H NMR spectra of low-spin iron(III) porphyrin radical cations taken in CD_2Cl_2 solution at 223 K. (a) $[Fe(TEtP^{\bullet})(HIm)_2]^+$ together with the expanded spectrum. (b) $[Fe(T^iPrP^{\bullet})(2\text{-}MeIm)_2]^+$. Adapted from Ref. [90].

from 2.4 to 232.6 ppm upon one-electron oxidation, which is a clear indication that the radical spin is in the a_{2u} orbital. Thus, the large upfield shift of pyrrole-H and downfield shift of *meso* α-H signals suggest that $[Fe(TRP^{\bullet})L_2]^{2+}$ adopt the same electronic structure as that of $[Fe(TArP^{\bullet})L_2]^{2+}$. It is known that highly ruffled low-spin $[Fe(T^iPrP)L_2]^+$ shows the less common $(d_{xz}, d_{yz})^4(d_{xy})^1$ ground state in all the axial ligands examined [8,28,60]. In fact, $[Fe(T^iPrP)(HIm)_2]^+$ adopts the $(d_{xz}, d_{yz})^4(d_{xy})^1$ ground state in spite of the coordination of HIm; all the low-spin bis(imidazole) complexes except $[Fe(T^iPrP)(HIm)_2]^+$ exhibit the $(d_{xy})^2(d_{xz}, d_{yz})^3$ ground state [8]. However, on one-electron oxidation, the pyrrole-H signal moves from 0.6 to −20.4 ppm and the *meso* α-H signal moves from 16.5 to 42.4 ppm. The upfield shift of the pyrrole-H signal indicates that the $(d_{xy})^2(d_{xz}, d_{yz})^3$ ground state is stabilized relative to the $(d_{xz}, d_{yz})^4(d_{xy})^1$ ground state on one-electron oxidation [90].

3.3.2. Iron(III) with the $(d_{xz}, d_{yz})^4(d_{xy})^1$ electron configuration

Low-spin iron(III) complexes having axial ligand with low-lying π* orbitals such as ^{t}BuNC and/or highly ruffled porphyrin core such as T^{i}PrP adopt the less common $(d_{xz}, d_{yz})^4(d_{xy})^1$ ground state [8]. As mentioned in the previous section, the iron(III) ion in radical cationic $[Fe(T^iPrP^{\bullet})(HIm)_2]^{2+}$ adopts the $(d_{xy})^2(d_{xz}, d_{yz})^3$ ground state though the corresponding $[Fe(T^iPrP)(HIm)_2]^+$ shows the $(d_{xz}, d_{yz})^4(d_{xy})^1$ ground state. Thus, the $(d_{xy})^2(d_{xz}, d_{yz})^3$ ground state is stabilized relative to the $(d_{xz}, d_{yz})^4(d_{xy})^1$ ground state on one-electron oxidation of the porphyrin ring. This is understandable because a_{2u} orbital should be greatly stabilized by the electron removal. As a result, the interaction between the d_{xy} and a_{2u} orbital is weakened on going from $[Fe(Por)L_2]^+$ to $[Fe(Por^{\bullet})L_2]^{2+}$ (L is a neutral ligand) because of the increase in energy gap between the two interacting orbitals. Thus, in order to obtain $[Fe(Por^{\bullet})L_2]^{2+}$ with the $(d_{xz}, d_{yz})^4(d_{xy})^1$ ground state, $[Fe(Por)L_2]^+$ has to carry suitable axial ligand where the d_{xy} orbital is located far above the d_π orbitals. Needless to say, ^{t}BuNC is the best candidate to obtain such complex since almost all the low-spin porphyrin and porphyrin analogues carrying ^{t}BuNC exhibit the $(d_{xz}, d_{yz})^4(d_{xy})^1$ ground state; the only two examples showing the $(d_{xy})^2(d_{xz}, d_{yz})^3$ ground state are diazaporphyrin $[Fe(DAzP)(^tBuNC)_2]^+$ and highly saddled $[Fe(OETArP)(^tBuNC)_2]^+$ with electron withdrawing aryl groups at the *meso* positions [49,64].

Ikezaki et al. prepared a series of $[Fe(TMP^{\bullet})L_2]^{2+}$ (L = HIm, 4,5-Cl_2Im, and ^{t}BuNC) by the addition of axial ligands(L) to the CD_2Cl_2 solution of Fe(TMP)ClO_4 at 195 K [91]. Fig. 9 shows the ^{1}H NMR spectra of these complexes taken at 173 K. The ^{1}H NMR spectrum of $[Fe(TMP^{\bullet})(HIm)_2]^{2+}$ shows clearly that the complex has low-spin $(d_{xy})^2(d_{xz}, d_{yz})^3$ type iron(III) with a_{2u} porphyrin radical cation; the chemical shifts of the pyrrole-H and *m*-H signals are −70.8 and 65.7 ppm, respectively, at 173 K. If axial HIm is replaced by 4,5-Cl_2Im, the pyrrole-H and *m*-H signals shift to ca. −26 and 24 ppm, respectively, as shown in Fig. 9(b); these signals split into several lines at this temperature due to the slow rotation of 4,5-Cl_2Im ligand. Thus, the isotropic shifts are greatly reduced on going from $[Fe(TMP^{\bullet})(HIm)_2]^{2+}$ to $[Fe(TMP^{\bullet})(4,5\text{-}Cl_2Im)_2]^{2+}$. In the case of $[Fe(TMP^{\bullet})(^tBuNC)_2]^{2+}$, all the signals are observed in a so called diamagnetic region, from 4.7 to 6.5 ppm in this case, as shown in Fig. 9(c). The effective magnetic moment of this complex is 0.45 μ_B at 173 K. The ^{1}H NMR chemical shifts of both neutral $[Fe(TMP)L_2]^+$ and radical cationic $[Fe(TMP^{\bullet})L_2]^{2+}$ are listed in Table 7. In neutral $[Fe(TMP)L_2]^+$, the pyrrole-H signal moves downfield from −16.8 to −9.4, and then to 7.1 ppm at 298 K as the axial ligand changes from HIm to 4,5-Cl_2Im, and then to ^{t}BuNC. The results indicate the change in electronic ground state from $(d_{xy})^2(d_{xz}, d_{yz})^3$ to $(d_{xz}, d_{yz})^4(d_{xy})^1$. Similar tendency is observed in radical cationic $[Fe(TMP^{\bullet})L_2]^{2+}$; the pyrrole-H signal moves downfield from −53.2 to −25.6, and then to 4.6 ppm. The results suggest that $[Fe(TMP^{\bullet})(HIm)_2]^{2+}$ and $[Fe(TMP^{\bullet})(^tBuNC)_2]^{2+}$ adopt the $(d_{xy})^2(d_{xz}, d_{yz})^3$ and the $(d_{xz}, d_{yz})^4(d_{xy})^1$ ground state, respectively. Diamagnetic nature of $[Fe(TMP^{\bullet})(^tBuNC)_2]^{2+}$ can then be explained in terms of the strong antiferromagnetic coupling between half-occupied d_{xy} and half-occupied a_{2u} orbital in a ruffled porphyrin framework. Since $[Fe(TMP^{\bullet})(4,5\text{-}Cl_2Im)_2]^{2+}$ exists as a mixture of the complexes with the $(d_{xy})^2(d_{xz}, d_{yz})^3$ and $(d_{xz}, d_{yz})^4(d_{xy})^1$ ground state, the pyrrole-H signal appears just between the corresponding signals of $[Fe(TMP^{\bullet})(HIm)_2]^{2+}$ and $[Fe(TMP^{\bullet})(^tBuNC)_2]^{2+}$. As mentioned, the pyrrole-H and *m*-H signals of $[Fe(TMP^{\bullet})(^tBuNC)_2]^{2+}$ appear at 4.7 and 6.5 ppm at 173 K, which are by 4.2 and 0.8 ppm more upfield than the corresponding signals of diamagnetic $[Co(TMP)(^tBuNC)_2]^+$. Similarly, $[Fe(TMP^{\bullet})(^tBuNC)_2]^{2+}$ shows the *meso*-C signal at 160 ppm at 173 K, which is by 42 ppm more downfield than the corresponding signal of diamagnetic $[Co(TMP)(^tBuNC)_2]^+$. Fig. 10(a) shows the Curie plots of the *m*-H and pyrrole-H signals of the three complexes. Clearly, the temperature dependence of the chemical shifts decreases on going from the HIm to the 4,5-Cl_2Im, and then to the ^{t}BuNC complex. The Curie plot of the *meso*-C signal of $[Fe(TMP^{\bullet})(^tBuNC)_2]^{2+}$ given in Fig. 10(b) exhibits a small downfield shift at higher temperature. These results indicate that $[Fe(TMP^{\bullet})(^tBuNC)_2]^{2+}$ adopts the S = 0 ground state with a small contribution from the thermally accessible excited state which is paramagnetic. Increase in radical cationic nature of the ^{t}BuNC complex can most explicitly be seen in the temperature dependence of the half-height width of the *meso*-C signal. As shown in Fig. 10(b), it increases drastically from 84 Hz at

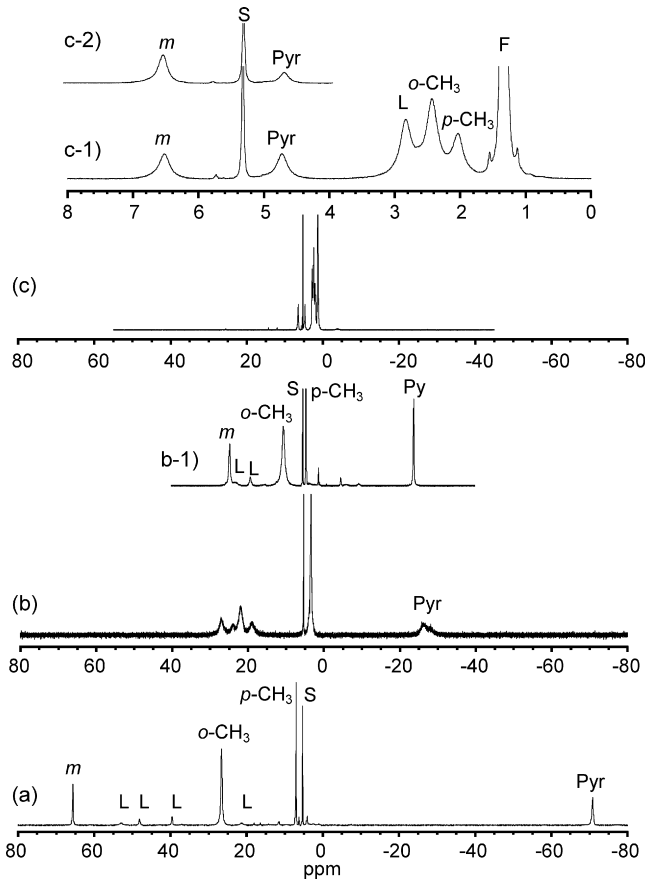

Fig. 9. (a) ^{1}H NMR spectrum of $[Fe(TMP^{\bullet})(HIm)_2]^{2+}$ taken in CD_2Cl_2 solution at 173 K. S and L indicate the signals for solvent and coordinated ligand. (b) ^{1}H NMR spectrum of $[Fe(TMP^{\bullet})(4,5\text{-}Cl_2Im)_2]^{2+}$ taken in CD_2Cl_2 solution at 173 K. The same sample taken at 253 K is given in inset (b-1). (c) ^{1}H NMR spectrum of $[Fe(TMP^{\bullet})(^tBuNC)_2]^{2+}$ taken in CD_2Cl_2 solution at 173 K. Inset (c-1) shows the 0-8 ppm region where L and F are the *tert*-butyl signals for coordinated and free ^{t}BuNC. Inset (c-2) shows the spectrum obtained from the pyrrole-d_8 complex. Adapted from Ref. [91].

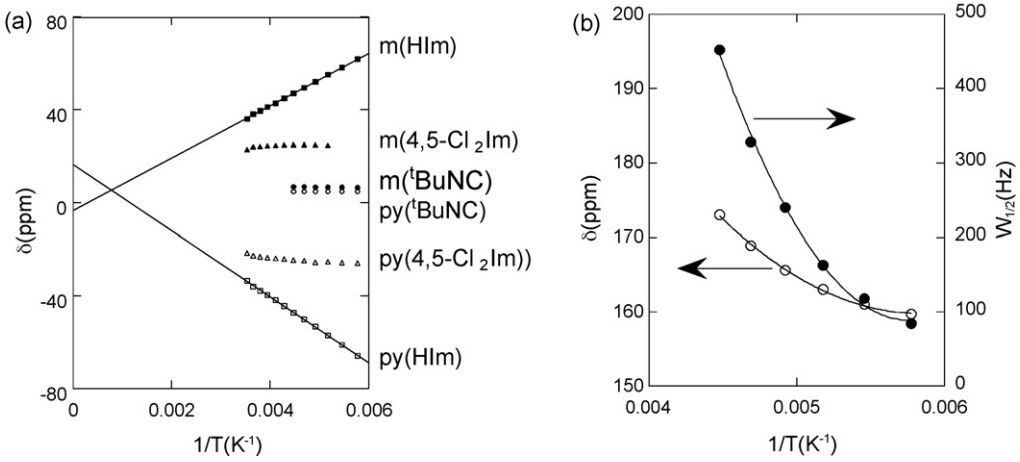

Fig. 10. (a) Curie plots of the *meta* and pyrrole-H chemical shifts of $[Fe(TMP^{\bullet})L_2]^{2+}$. (b) Curie plots (○) and temperature dependence of the half-height width (●) of the *meso*-C signal of $[Fe(TMP^{\bullet})(^tBuNC)_2]^{2+}$. Adapted from Ref. [91].

173 K to 452 Hz at 223 K, supporting the increase in population of the paramagnetic species.

4. Iron(IV) porphyrins

4.1. Iron(IV) complexes with Fe=O bond

Iron(IV) porphyrins are quite unstable and difficult to obtain. Balch and co-workers reported the first example of Fe^{IV}=O complex, [(Fe=O)(3-MeTPP)(1-MeIm)], by the addition of 1-MeIm to the peroxo-bridged dimer (3-MeTPP)FeO–OFe(3-MeTPP) [92,93]. The iron(IV) oxidation state has been confirmed by the solution magnetic moment which is $2.9 \pm 0.1\ \mu_B$ at 221 K and is invariant down to 183 K. The temperature dependence of the paramagnetic shift of each signal strictly follows the Curie law over al large temperature range. The complex decomposes to the μ-oxo dimer above 243 K at an appreciable rate. Hence the iron ion of this complex exists in well defined paramagnetic, noninteracting states [92]. Thermal decomposition of the peroxo-bridged dimer of sterically hindered TMP, (TMP)FeO–OFe(TMP), yields five-coordinate complex (Fe=O)(TMP) [94,95]. Similarly, thermal decomposition of alkylperoxo complex, Fe(TMP)(OO^{t}Bu), produces (Fe=O)(TMP) [96]. Later, Groves et al. reported the convenient preparative method for (Fe^{IV}=O)(TMP); the ligand metathesis of iron(III) radical cation, $Fe(TMP^{\bullet})(ClO_4)_2$, over moist basic alumina [97]. The ^{1}H NMR chemical shifts of various Fe=O complexes are listed in Table 8 [98,99]. As is revealed from the data in Table 8, the isotropic shift of each signal in both five- and six-coordinate Fe=O complexes is quite small. Since these complexes adopt the S = 1 $(d_{xy})^2(d_{xz}, d_{yz})^2$ ground state, one can expect that the pyrrole-H signals should appear extremely upfield due to the interaction between half-filled iron d_π and filled porphyrin $3e_g$ orbitals as in the case of the S = 3/2 iron(III) complexes such as Fe(TPP)[$Ag(Br_6CB_{11}H_6)_2$]; the chemical shift of the pyrrole-H signal reaches as much as −62.0 ppm at 298 K [10]. Theoretical calculations have revealed that most of the unpaired electrons in the Fe=O complexes are localized on the axial part, i.e. iron and oxygen atoms, and that the amount of the total spin density on the porphyrin ring is negligibly small [100,101]. Thus, the theoretical study explains why the isotropic shifts of the peripheral proton signals in the Fe=O complexes are negligibly small in spite of the presence of two unpaired electrons in the d_π orbitals.

4.2. Iron(IV) complexes without Fe=O bond

While there are ample examples of iron(IV) complexes with Fe=O bond, the iron(IV) complexes without Fe=O bond are quite rare. Only example is bis-methoxo complex, $[Fe(TMP)(OMe)_2]$, which is prepared by the addition of methoxide to the iron(III) porphyrin radical cation, $Fe(TMP^{\bullet})(ClO_4)_2$, as shown in Eq. (2) [84].

$$Fe^{III}(TMP^{\bullet})(ClO_4)_2 + 2MeO^- \rightleftarrows [Fe^{IV}(TMP)(OMe)_2] + 2ClO_4^- \quad (2)$$

The electronic structure of $[Fe(TMP)(OMe)_2]$ has been examined by various spectroscopic methods. The ^{1}H NMR chemical shifts of this complex are listed in Table 8. The characteristic feature is that the pyrrole-H signal appears at an extremely upfield position, $\delta = -37.5$ ppm at 195 K, while the other signals such as *o*-CH_3, *m*-H, and *p*-CH_3 are quite close to their diamagnetic positions. The effective magnetic moment μ_{eff} is $2.9 \pm 0.2\ \mu_B$ between 229 and

Table 8
^{1}H NMR Chemical Shifts of Iron(IV) porphyrin complexes[a].

Complexes	T (K)	Pyrrole	*o*-H	*m*-H	*p*-H	Ref.
(Fe=O)(TMP)	195	5.85	(3.40, 1.05)	6.75, 6.20	(2.70)	[97]
	203	8.4	(3.3, –)	6.4, 6.0	(2.6)	[94]
	273	7.30	(2.80, 1.25)	6.35,6.70	(2.60)	[97]
(Fe=O)(3-MeTPP)(1-MeIm)	200	5.1	8.7	7.8, –	7.8	[92]
(Fe=O)(TMP)(1-MeIm)	213	–	(3 6, –)	7.5, –	(2 74)	[94]
	243	4.6	(3.2, 1.6)	7.4, –	(2.67)	[94]
(Fe=O)(TMP)(OMe-d_3)	243	0.1, −4.1	(1.5, –)	–	(2.7)	[98]
(Fe=O)(TPP)(L)[b]	197	1.2	9.1	7.9	8.3	[99]
(Fe=O)(TPP)(1-MeIm)	193	5.05	9.2, –	7.9, –	7.9	[94]
$Fe(TMP)(OMe)_2$	195	−37.5	(2.4)	7.72	(2.86)	[84]

[a] Data in parentheses are the chemical shifts of the methyl signals.
[b] Chemical shifts are obtained from Fig. 1 of Ref. [99]. Axial ligand(L) is not specified.

193 K in CH_2Cl_2 solution. Thus, the complex is best described as iron(IV) porphyrin with the S = 1 ground state, which is further verified by the Mössbauer and EXAFS data [102]. Because of the absence of the Fe=O bond, the unpaired electrons in the d_{xz} and d_{yz} orbitals delocalize to the porphyrin ring by the interaction with the filled $3e_g$ orbitals to induce large upfield shift of the pyrrole-H signal. The ^{13}C NMR study further reveals that [Fe(TMP)$(OCD_3)_2$] has negligibly small spin density at the *meso*-carbon atoms because the *meso*-C signal appears at 64.3 ppm at 213 K; the *meso*-C signal of low-spin [Fe(T^{n}PrP)$(HIm)_2]^+$ with the $(d_{xy})^2(d_{xz}, d_{yz})^3$ ground state appears at 73.1 ppm as listed in Table 2 [48]. [Fe(TMP)$(OMe\text{-}d_3)_2$] is produced together with the two-electron oxidized product, [(Fe=O)(TMP)]$^+$, by the oxidation of Fe(TMP)(ClO_4) with iodosobenzene or dimethyldioxolane in mixed CD_2Cl_2 and CD_3OD solution• [84,103,104].

It has been expected that the addition of strong anionic ligands to the solution of iron(III) porphyrin radical cation could produce iron(IV) porphyrin as in the case of [Fe(TMP)$(OMe)_2$]. Among various anionic ligands, F^- should be a suitable ligand since it is highly ranked in a magnetochemical series postulated by Reed and co-workers [10,11,105]. In fact, the electrochemical oxidation of Fe(TPP)$F_2{}^-$ is unique in the sense that the first oxidation wave is +0.68 V [106,107]. Since the first oxidation wave for the most five-coordinate iron(III) porphyrins is ca. +1.1 V, the oxidation wave has been suggested to be due to an iron-centered oxidation to form iron(IV) species, Fe(TPP)F_2. However, the complex is too unstable to obtain the NMR spectrum. Density functional study has also predicted that one-electron oxidation of Fe(Por)$F_2{}^-$ should form iron(IV) porphyrin, Fe(Por)F_2, rather than iron(III) porphyrin radical cation [108]. Recently, Ghosh and Taylor reported that ab initio CASPT2 calculations favor a high-spin porphyrin radical cation as the ground state by a significant energetic margin over iron(IV) porphyrin [109,110]. Thus, the electronic structure of one-electron oxidized product of high-spin Fe(TPP)$F_2{}^-$ is still ambiguous and further experimental study should be done.

5. Conclusion

Relationships between NMR chemical shifts and electronic structures of one-electron oxidized products of iron(III) porphyrins such as iron(III) porphyrin radical cations and iron(IV) porphyrins have been described. The former can be classified into four types depending on the spin states and electron configurations of the iron(III) ions. They are, (A) high-spin iron(III), (B) intermediate-spin or mixed high- and intermediate-spin iron(III), (C) low-spin $(d_{xy})^2(d_{xz}, d_{yz})^3$ type iron(III), and (D) low-spin $(d_{xz}, d_{yz})^4(d_{xy})^1$ type iron(III). The radical spin on the porphyrin is either in the a_{2u} or a_{1u} orbital. In the case of type (A) complexes, the a_{2u} radical spin can antiferromagnetically interact with the high-spin iron(III) in five-coordinate domed C_{4v} complexes to form the S = 2 spin state as exemplified by Fe^{III}(TPP•)Cl$^+$. The antiferromagnetic coupling is clearly seen in the NMR spectrum where the *meso*-C and *m*-H signals appear at extremely upfield positions, i.e. −1910 and −12.4 ppm, respectively. By contrast, the a_{1u} radical exhibits little interaction with the iron spins as exemplified by the ^1H NMR spectrum of Fe^{III}(OEP•)Cl$^+$; the isotropic shifts of both the *meso*-H and CH_2 signals rather decrease on one-electron oxidation. However, the possibility still remains that Fe^{III}(OEP•)Cl$^+$ has radical spin in the a_{2u} orbital and that the radical spin antiferromagnetically couples with iron spins. In the case of type (B) complexes such as Fe(TPP•)$(ClO_4)_2$, the field strengths of the axial ligands are generally very weak. If the complexes have planar structure as in the case of Fe(TPP•)$(ClO_4)_2$, the radical spin should exhibit little interactions with the iron spins. Consequently, a large positive spin is concentrated on the *meso*-C and pyrrole-N atoms in the a_{2u} radical and causes large downfield shift of the *m*-H signal. As for the highly deformed Fe(Por•)$(ClO_4)_2$, the interaction is expected between radical spin and iron spins though no examples have ever been reported. Type (C) complexes such as Fe(TPP•)$(HIm)_2{}^{2+}$ have iron spin in one of the d_π orbitals which are orthogonal to both the a_{1u} and a_{2u} orbitals regardless of the porphyrin structure. Thus, the radical spin behaves independently and shifts the *m*-H signal to the downfield position. Type (D) complex, Fe^{III}(TMP•)$(^t$BuNC$)_2{}^{2+}$, has iron spin in the d_{xy} orbital. Thus, a strong antiferromagnetic coupling is expected between the radical spin and the iron spin in a presumably ruffled porphyrin core to form the S = 0 complex. In fact, this complex exhibits a well-resolved NMR spectrum where all the signals are in a so-called diamagnetic region though the effective magnetic moment is not completely zero, i.e. 0.45 μ_B at 173 K. A contribution from the thermally accessible excited state is considered to be one of the reasons for the small paramagnetism.

There are two types of iron(IV) complexes both of which adopt the $(d_{xy})^2(d_{xz}, d_{yz})^2$ configuration. One is five- or six-coordinate Fe^{IV}=O complexes signified as (Fe^{IV}=O)(Por) or (Fe^{IV}=O)(Por)L and the other is six-coordinate Fe^{IV}(Por)X_2. In the former complexes, the iron spins are localized on the iron-oxygen bond. Thus, the spin densities on the porphyrin carbon and nitrogen atoms are fairly small. Consequently, the peripheral substituents exhibit very

Table 9
Electronic structure and NMR characteristics of one-electron oxidized complexes of iron(III) porphyrins[a].

Complexes	T (K)	Oxidation state of iron	Spin state of iron	Porphyrin	NMR (CD_2Cl_2, δ ppm)					μ_{eff} (μ_B)[b]	Ref.
					Pyrrole-H	*o*-H	*m*-H	*p*-H	*meso*-C		
Fe^{III}(TPP•)Cl$^+$	298	Fe(III)	S = 5/2	a_{2u} radical cation	66.1	37.6, 34.4	−12.4	29.5	−1910	5.1	[70,81]
Fe^{III}(TPP•)$ClO_4)_2$	298	Fe(III)	S = 5/2, S = 3/2	a_{2u} radical cation	31.4	−19.3	34.7	−12.9		4.4–5.2[c]	[71]
[Fe^{III}(TPP•)$(HIm)_2]^{2+}$	235	Fe(III)	S = 1/2(d_π)[d]	a_{2u} radical cation	−40.1	−31.7	30.4	−22.1		2.8[e]	[86]
[Fe^{III}(TMP•)$(HIm)_2]^{2+}$	213	Fe(III)	S = 1/2(d_π)[d]	a_{2u} radical cation	−53.2	(20.1)	52.1	(7.0)			[91]
[Fe^{III}(TMP•)$(4,5^-Cl_2Im)_2]^{2+}$	213	Fe(III)	S = 1/2(d_π, d_{xy})[f]	a_{2u} radical cation	−25.6	n.d.	24.8	(4.0)			[91]
[Fe^{III}(TMP•)$(^t$BuNC$)_2]^{2+}$	213	Fe(III)	S = 1/2(d_{xy})[d]	a_{2u} radical cation	4.7	(2.4)	6.5	(2.0)	160[g]	0.45[h]	[91]
(Fe^{IV}=O)(TMP)	195	Fe(IV)	S = 1($d_\pi{}^2$)[i]	Neutral	5.9	(3.4, 1.1)	6.8, 6.2	(2.6)		2.9[j]	[97]
Fe^{IV}(TMP)$(OMc)_2$	195	Fe(IV)	S = 1($d_\pi{}^2$)[i]	Neutral	−37.5	(2.4)	7.7	(2.9)	64	2.9	[84]

[a] Data in parentheses are the chemical shifts of the methyl signals.
[b] Solution magnetic moments determined by the Evans method.
[c] Solid sample shows 6.5 μ_B [73].
[d] S = 1/2(d_π) and S = 1/2 (d_{xy}) indicate that the complex adopts the $(d_{xy})^2(d_{xz}, d_{yz})^3$ and $(d_{xz}, d_{yz})^4(d_{xy})^1$ ground state, respectively.
[e] The value obtained for analgous [Fe(4-OCH_3TPP•)$(HIm)_2]^{2+}$ [86].
[f] S = 1/2(d_{xy}, d_π) indicates that the complex exists as a mixture of two isomers adopting the $(d_{xy})^2(d_{xz}, d_{yz})^3$ and $(d_{xz}, d_{yz})^4(d_{xy})^1$ ground state.
[g] The chemical shift obtained at 173 K [91].
[h] The value obtained at 173 K.
[i] S = 1(d_π)^2 indicates that the complex shows the $(d_{xy})^2(d_{xz}, d_{yz})^2$ ground state.
[j] The μ_{eff} value obtained for (Fe=O) (3-MeTPP)(1-MeIm) [92].

broad signals close to their diamagnetic positions. There is only one example classified as $Fe^{IV}(Por)X_2$, i.e. $Fe^{IV}(TMP)(OMe)_2$. As expected, this complex exhibits the pyrrole-H signal at an extraordinary upfield positions due to the d_π–$3e_g$ interactions. In Table 9 are given the NMR characteristics of eight typical complexes showing either iron(III) porphyrin radical or iron(IV) porphyrin. As is clear from Table 9, only a limited number of the iron(IV) complexes are reported.

There is no example showing the diamagnetic (S = 0) iron(IV) complexes which are possible if the energy levels between the d_{xy} and d_π orbitals are reversed. Similarly, there is no high-spin (S = 2) iron(IV) complexes. The synthesis, characterization, and the study on reactivity of these complexes are the challenge in coordination chemistry and would be useful for further understanding the biological processes that heme proteins are involved.

References

[1] J.T. Groves, K. Shalyaev, J. Lee, in: K.M. Kadish, K.M. Smith, R. Guilard (Eds.), The Porphyrin Handbook, vol. 4, Academic Press, San Diego, CA, 2000, p. 17 (Chapter 27).
[2] R. Weiss, A. Gold, A.X. Trautowein, J. Terner, in: K.M. Kadish, K.M. Smith, R. Guilard (Eds.), The Porphyrin Handbook, vol. 4, Academic Press, San Diego, CA, 2000, p. 65 (Chapter 29).
[3] Y. Watanabe, in: K.M. Kadish, K.M. Smith, R. Guilard (Eds.), The Porphyrin Handbook, vol. 4, Academic Press, San Diego, CA, 2000, p. 97 (Chapter 30).
[4] M. Costas, M.P. Mehn, M.P. Jensen, L. Que Jr., Chem. Rev. 104 (2004) 939.
[5] J. Conradie, I. Wasbotten, A. Ghosh, J. Inorg. Biochem. 100 (2006) 502.
[6] F.A. Walker, in: K.M. Kadish, K.M. Smith, R. Guilard (Eds.), The Porphyrin Handbook, vol. 5, Academic Press, San Diego, 2000, p. 81 (Chapter 36).
[7] W.R. Scheidt, in: K.M. Kadish, K.M. Smith, R. Guilard (Eds.), The Porphyrin Handbook, vol. 3, Academic Press, San Diego, 2000, p. 49 (Chapter 16).
[8] M. Nakamura, Coord. Chem. Rev. 250 (2006) 2271.
[9] W.R. Scheidt, C.A. Reed, Chem. Rev. 81 (1981) 543.
[10] C.A. Reed, F. Guiset, J. Am. Chem. Soc. 118 (1996) 3281.
[11] D.R. Evans, C.A. Reed, J. Am. Chem. Soc. 122 (2000) 4660.
[12] T. Ikeue, T. Saitoh, T. Yamaguchi, Y. Ohgo, M. Nakamura, M. Takahashi, M. Takeda, Chem. Commun. (2000) 1989.
[13] J.-P. Simonato, J. Pécaut, L.L. Pape, J.-L. Oddou, C. Jeandey, M. Shang, W.R. Scheidt, J. Wojaczyński, S. Wołowiec, L. Latos-Grażyński, J.-C. Marchon, Inorg. Chem. 39 (2000) 3978.
[14] M. Nakamura, T. Ikeue, Y. Ohgo, M. Takahashi, M. Takeda, Chem. Commun. (2002) 1198.
[15] T. Ikeue, Y. Ohgo, T. Yamaguchi, M. Takahashi, M. Takeda, M. Nakamura, Angew. Chem. Int. Ed. 40 (2001) 2617.
[16] Y. Ohgo, T. Ikeue, M. Nakamura, Inorg. Chem. 41 (2002) 1698.
[17] T. Ikeue, Y. Ohgo, O. Ongayi, M.G.H. Vicente, M. Nakamura, Inorg. Chem. 42 (2003) 5560.
[18] Y. Ohgo, T. Ikeue, M. Takahashi, M. Takeda, M. Nakamura, Eur. J. Inorg. Chem. (2004) 798.
[19] K. Nakamura, A. Ikezaki, Y. Ohgo, T. Ikeue, S. Neya, M. Nakamura, Inorg. Chem. 47 (2008) 10299.
[20] W.R. Scheidt, D.K. Geiger, K.J. Haller, J. Am. Chem. Soc. 104 (1982) 495.
[21] M.K. Ellison, H. Nasri, Y.-M. Xia, J.-C. Marchon, C.E. Schulz, P.G. Debrunner, W.R. Scheidt, Inorg. Chem. 36 (1997) 4804.
[22] S. Neya, M. Tsubaki, H. Hori, T. Yonetani, N. Funasaki, Inorg. Chem. 40 (2001) 1220.
[23] S. Neya, C.K. Chang, D. Okuno, T. Hoshino, M. Hata, N. Funasaki, Inorg. Chem. 44 (2005) 1193.
[24] Y. Ohgo, Y. Chiba, D. Hashizume, H. Uekusa, T. Ozeki, M. Nakamura, Chem. Commun. (2006) 1935.
[25] S. Neya, A. Takahashi, H. Ode, T. Hoshino, M. Hata, A. Ikezaki, Y. Ohgo, M. Takahashi, H. Hiramatsu, T. Kitagawa, Y. Furutani, H. Kandori, N. Funasaki, M. Nakamura, Eur. J. Inorg. Chem. (2007) 3188.
[26] S. Neya, A. Takahashi, H. Ode, T. Hoshino, A. Ikezaki, Y. Ohgo, M. Takahashi, Y. Furutani, V.A. Lórenz-Fonfría, H. Kandori, H. Hiramatsu, T. Kitagawa, J. Teraoka, N. Funasaki, M. Nakamura, Bull. Chem. Soc. Jpn. 81 (2008) 136.
[27] F.A. Walker, Inorg. Chem. 42 (2003) 4526.
[28] M. Nakamura, Y. Ohgo, A. Ikezaki, J. Inorg. Biochem. 102 (2008) 433.
[29] T. Sakai, Y. Ohgo, T. Ikeue, M. Takahashi, M. Takeda, M. Nakamura, J. Am. Chem. Soc. 125 (2003) 13028.
[30] G.N. La Mar, F.A. Walker, in: D. Dolphin (Ed.), The Porphyrin, vol. 4, Academic Press, New York, 1979, p. 61 (Chapter 2).
[31] F.A. Walker, Chem. Rev. 104 (2004) 589.
[32] H.M. Goff, in: A.B.P. Lever, H.B. Gray (Eds.), Physical Bioinorganic Chemistry Series 1, Iron Porphyrins, I, Addison-Wesley, Reading, MA, 1983, p. 237 (Chapter 4).
[33] F.A. Walker, U. Simonis, in: L.J. Berliner, J. Reuben (Eds.), NMR of Paramagnetic Molecules, vol. 12, Plenum Press, New York, 1993, p. 133.
[34] I. Bertini, C. Luchinat, in: A.B.P. Lever (Ed.), NMR of Paramagnetic Substances, Coordination Chemistry Reviews, vol. 150, Elsevier, Amsterdam, 1996, p. 29.
[35] L.-J. Ming, in: L. Que Jr. (Ed.), Physical Method in Bioinorganic Chemistry, University Science Books, Sausalito, CA, 2000, p. 375 (Chapter 8).
[36] W.R. Scheidt, Y.J. Lee, Struct. Bonding (Berlin) 64 (1987) 1.
[37] K.M. Barkigia, M.D. Berber, J. Fajer, C.J. Medforth, M.W. Renner, K.M. Smith, J. Am. Chem. Soc. 112 (1990) 8851.
[38] W. Jentzen, X.Z. Song, J.A. Shelnutt, J. Phys. Chem. B 101 (1997) 1684.
[39] J.A. Shelnutt, X.-Z. Song, J.-G. Ma, S.-L. Jia, W. Jentzen, C.J. Medforth, Chem. Soc. Rev. 27 (1998) 31.
[40] M.O. Senge, in: K.M. Kadish, K.M. Smith, R. Guilard (Eds.), The Porphyrin Handbook, vol. 1, Academic Press, San Diego, CA, 2000, p. 239 (Chapter 6).
[41] R.-J. Cheng, P.-Y. Chen, T. Lovell, T. Liu, L. Noodleman, D.A. Case, J. Am. Chem. Soc. 125 (2003) 6774.
[42] J. Conradie, A. Ghosh, J. Phys. Chem. B 107 (2003) 6486.
[43] M.K. Safo, G.P. Gupta, C.T. Watson, U. Simonis, F.A. Walker, W.R. Scheidt, J. Am. Chem. Soc. 114 (1992) 7066.
[44] M.K. Safo, F.A. Walker, A.M. Raitsimring, W.P. Walters, D.P. Dolata, P.G. Debrunner, W.R. Scheidt, J. Am. Chem. Soc. 116 (1994) 7760.
[45] M.R. Cheesman, F.A. Walker, J. Am. Chem. Soc. 118 (1996) 7373.
[46] M.W. Renner, K.M. Barkigia, Y. Zhang, C.J. Medforth, K.M. Smith, J. Fajer, J. Am. Chem. Soc. 116 (1994) 8582.
[47] J. Shao, E. Steene, B.M. Hoffman, A. Ghosh, Eur. J. Inorg. Chem. (2005) 1609.
[48] T. Ikeue, Y. Ohgo, T. Saitoh, M. Nakamura, H. Fujii, M. Yokoyama, J. Am. Chem. Soc. 122 (2000) 4068.
[49] Y. Ohgo, S. Neya, H. Uekusa, M. Nakamura, Chem. Commun. (2006) 4590.
[50] G. Simonneaux, F. Hindre, M. Le Plouzennec, Inorg. Chem. 28 (1989) 823.
[51] C. Gèze, N. Legrand, A. Bondon, G. Simonneaux, Inorg. Chim. Acta 195 (1992) 73.
[52] F.A. Walker, H. Nasri, I. Turowska-Tyrk, K. Mohanrao, C.T. Watson, N.V. Shokhirev, P.G. Debrunner, W.R. Scheidt, J. Am. Chem. Soc. 118 (1996) 12109.
[53] S. Wołowiec, L. Latos-Grażyński, M. Mazzanti, J.-C. Marchon, Inorg. Chem. 36 (1997) 5761.
[54] M. Nakamura, T. Ikeue, H. Fujii, T. Yoshimura, J. Am. Chem. Soc. 119 (1997) 6284.
[55] M.-A. Pilard, M. Guillemot, L. Toupet, J. Jordanov, G. Simonneaux, Inorg. Chem. 36 (1997) 6307.
[56] S. Wołowiec, L. Latos-Grażyński, D. Toronto, J.-C. Marchon, Inorg. Chem. 37 (1998) 724.
[57] M. Nakamura, T. Ikeue, H. Fujii, T. Yoshimura, K. Tajima, Inorg. Chem. 37 (1998) 2405.
[58] K.T. Moore, J.T. Fletcher, M.J. Therien, J. Am. Chem. Soc. 121 (1999) 5196.
[59] G. Simonneaux, V. Schünemann, C. Morice, L. Carel, L. Toupet, H. Winkler, A.X. Trautwein, F.A. Walker, J. Am. Chem. Soc. 122 (2000) 4366.
[60] T. Ikeue, Y. Ohgo, T. Saitoh, T. Yamaguchi, M. Nakamura, Inorg. Chem. 40 (2001) 3423.
[61] A. Ikezaki, T. Ikeue, M. Nakamura, Inorg. Chim. Acta 335 (2002) 91.
[62] A. Ikezaki, M. Nakamura, Inorg. Chem. 41 (2002) 2761.
[63] A. Hoshino, Y. Ohgo, M. Nakamura, Inorg. Chem. 44 (2005) 7333.
[64] Y. Ohgo, A. Hoshino, T. Okamura, H. Uekusa, D. Hashizume, A. Ikezaki, M. Nakamura, Inorg. Chem. 46 (2007) 8193.
[65] R.-J. Cheng, S.-H. Chang, K.-C. Hung, Inorg. Chem. 46 (2007) 1948.
[66] H.M. Goff, E.T. Shimomura, M.A. Phillippi, Inorg. Chem. 22 (1983) 66.
[67] M. Nakamura, A. Hoshino, A. Ikezaki, T. Ikeue, Chem. Commun. 1862 (2003).
[68] A.Y. Alontaga, R.A. Bunce, A. Wilks, M. Rivera, Inorg. Chem. 45 (2006) 8876.
[69] M.A. Phillippi, E.T. Shimomura, H.M. Goff, Inorg. Chem. 20 (1981) 1322.
[70] M.A. Phillippi, H.M. Goff, J. Am. Chem. Soc. 104 (1982) 6026.
[71] A.D. Boersma, H.M. Goff, Inorg. Chem. 23 (1984) 1671.
[72] W.F. Scholz, C.A. Reed, Y.J. Lee, W.R. Scheidt, G. Lang, J. Am. Chem. Soc. 104 (1982) 6791.
[73] G. Buisson, A. Deronzier, E. Duée, P. Gans, J.-C. Marchon, J.-R. Regnard, J. Am. Chem. Soc. 104 (1982) 6793.
[74] P. Gans, G. Buisson, E. Duée, J.-C. Marchon, B.S. Erler, W.F. Scholz, C.A. Reed, J. Am. Chem. Soc. 108 (1986) 1223.
[75] M. Nakamura, Y. Kawasaki, Chem. Lett. 25 (1996) 805.
[76] A.L. Balch, L. Latos-Grażyński, B.C. Noll, L. Szterenberg, E.P. Zovinka, J. Am. Chem. Soc. 115 (1993) 11846.
[77] A. Nanthakumar, H.M. Goff, Inorg. Chem. 30 (1991) 4460.
[78] M. Nakamura, T. Yamaguchi, Y. Ohgo, Inorg. Chem. 38 (1999) 3126.
[79] M. Rivera, G.A. Caignan, Anal. Bioanal. Chem. 378 (2004) 1464.
[80] L.K. Hanson, C.K. Chang, M.S. Davis, J. Fajer, J. Am. Chem. Soc. 103 (1981) 663.
[81] A. Hoshino, M. Nakamura, Chem. Commun. (2005) 915.
[82] T. Sakai, Y. Ohgo, A. Hoshino, T. Ikeue, T. Saitoh, M. Takahashi, M. Nakamura, Inorg. Chem. 43 (2004) 5034.
[83] G.E. Toney, A. Gold, J. Savrin, L.W. Ter Haar, R. Sangaiah, W.E. Hatfield, Inorg. Chem. 23 (1984) 4350.
[84] J.T. Groves, R. Quinn, T.J. McMurry, M. Nakamura, G. Lang, B. Boso, J. Am. Chem. Soc. 107 (1985) 354.
[85] A. Ikezaki, M. Nakamura, Inorg. Chem. 41 (2002) 6225.
[86] H.M. Goff, M.A. Phillippi, J. Am. Chem. Soc. 105 (1983) 7567.
[87] M. Nakamura, J.T. Groves, Tetrahedron 44 (1988) 3225.
[88] M. Nakamura, N. Nakamura, Chem. Lett. 20 (1991) 1885.
[89] M. Nakamura, K. Tajima, K. Tada, K. Ishizu, N. Nakamura, Inorg. Chim. Acta 224 (1994) 113.
[90] T. Ikeue, Y. Ohgo, M. Nakamura, Chem. Commun. (2003) 220.
[91] A. Ikezaki, H. Tukada, M. Nakamura, Chem. Commun. (2008) 2257.
[92] D.-H. Chin, A.L. Balch, G.N. La Mar, J. Am. Chem. Soc. 102 (1980) 1446.
[93] D.-H. Chin, G.N. La Mar, A.L. Balch, J. Am. Chem. Soc. 102 (1980) 5945.

[94] A.L. Balch, Y.-W. Chan, R.-J. Cheng, G.N. La Mar, L. Latos-Grazynski, M.W. Renner, J. Am. Chem. Soc. 106 (1984) 7779.
[95] A.L. Balch, G.N. La Mar, L. Latos-Grazynski, M.W. Renner, V. Thanabal, J. Am. Chem. Soc. 107 (1985) 3003.
[96] R.D. Arasasingham, C.R. Cornman, A.L. Balch, J. Am. Chem. Soc. 111 (1989) 7800.
[97] J.T. Groves, Z. Gross, M.K. Stern, Inorg. Chem. 33 (1994) 5065.
[98] A.L. Balch, C.R. Cornman, L. Latos-Grażyński, M.W. Renner, J. Am. Chem. Soc. 114 (1992) 2230.
[99] K. Shin, H.M. Goff, J. Am. Chem. Soc. 109 (1987) 3140.
[100] G.H. Loew, C.J. Kert, L.M. Hjelmeland, R.F. Kirchner, J. Am. Chem. Soc. 99 (1977) 3534.
[101] A. Dey, A. Ghosh, J. Am. Chem. Soc. 124 (2002) 3206.
[102] J.E. Penner-Hahn, T.J. McMurry, M. Renner, L. Latos-Grażyński, K.S. Eble, I.M. Davis, A.L. Balch, J.T. Groves, J.H. Dawson, K.O. Hodgson, J. Biol. Chem. 258 (1983) 12761.
[103] J.T. Groves, R.C. Haushalter, M. Nakamura, T.E. Nemo, B.J. Evans, J. Am. Chem. Soc. 103 (1981) 2884.
[104] S. Wołowiec, L. Latos-Grażyński, Inorg. Chem. 37 (1998) 2984.
[105] C.A. Reed, Inorg. Chim. Acta 263 (1997) 95.
[106] D.L. Hickman, H.M. Goff, Inorg. Chem. 22 (1983) 2787.
[107] D.L. Hickman, A. Nanthakumar, H.M. Goff, J. Am. Chem. Soc. 110 (1988) 6384.
[108] D.H. Jones, A.S. Hinman, T. Ziegler, Inorg. Chem. 32 (1993) 2092.
[109] A. Ghosh, B.J. Persson, P.R. Taylor, J. Biol. Inorg. Chem. 8 (2003) 507.
[110] A. Ghosh, P.R. Taylor, J. Chem. Theory Comput. 1 (2005) 597.
[111] J. Mispelter, M. Momenteau, J.-M. Lhoste, J. Chem. Soc. Chem. Commun. (1979) 808.
[112] J. Mispelter, M. Momenteau, J.-M. Lhoste, J. Chem. Soc. Dalton Trans. (1981) 1729.
[113] A. Ikezaki, unpublished results.